

## Closure statistics in radio interferometric data

LINDY BLACKBURN,<sup>1,2</sup> DOMINIC W. PESCE,<sup>1,2</sup> MICHAEL D. JOHNSON,<sup>1,2</sup> MACIEK WIELGUS,<sup>1,2</sup>  
ANDREW A. CHAEL,<sup>3,4</sup> PIERRE CHRISTIAN,<sup>5</sup> AND SHEPERD S. DOELEMAN<sup>1,2</sup>

<sup>1</sup>*Center for Astrophysics | Harvard & Smithsonian, 60 Garden Street, Cambridge, MA 02138, USA*

<sup>2</sup>*Black Hole Initiative, Harvard University, 20 Garden Street, Cambridge, MA 02138, USA*

<sup>3</sup>*Princeton Center for Theoretical Science, Jadwin Hall, Princeton University, Princeton, NJ 08544, USA*

<sup>4</sup>*NASA Hubble Fellowship Program, Einstein Fellow*

<sup>5</sup>*University of Arizona, 933 North Cherry Avenue, Tucson, AZ 85721, USA*

### ABSTRACT

Interferometric visibilities, reflecting the complex correlations between signals recorded at antennas in an interferometric array, carry information about the angular structure of a distant source. While unknown antenna gains in both amplitude and phase can prevent direct interpretation of these measurements, certain combinations of visibilities called closure phases and closure amplitudes are independent of antenna gains and provide a convenient set of robust observables. However, these closure quantities have subtle noise properties and are generally both linearly and statistically dependent. These complications have obstructed the proper use of closure quantities in interferometric analysis, and they have obscured the relationship between analysis with closure quantities and other analysis techniques such as self calibration. We review the statistics of closure quantities, focusing on common pitfalls at low signal-to-noise due to the nonlinear propagation of statistical errors. We then develop a strategy for isolating and fitting to the independent degrees of freedom captured by the closure quantities through explicit construction of linearly independent sets of quantities along with their noise covariance in the Gaussian limit, and we demonstrate that model fits have biased posteriors when this covariance is ignored. Finally, we introduce a unified procedure for fitting to both closure information and partially calibrated visibilities, and we demonstrate both analytically and numerically the direct equivalence of inference based on closure quantities to that based on self calibration of complex visibilities with unconstrained antenna gains.

**Keywords:** techniques: interferometric — methods: data analysis — methods: statistical — techniques: high angular resolution

1. Introduction	2	5. Summary	15
2. Closure quantities and errors	2	A. Distributions due to thermal noise	18
2.1. Interferometric visibility and gain	2	A.1. Phase and amplitude distributions	18
2.2. Closure phase and closure amplitude	3	A.2. Log amplitude ensemble distribution	19
2.3. Statistical thermal noise	3	A.3. Quality of distribution approximations	22
2.4. Non-Gaussian errors at low S/N	4	B. Design and covariance matrix construction	22
3. Independence of closure quantities	5	B.1. Baseline phase and amplitude matrices	22
3.1. Closure covariance due to thermal noise	5	B.2. Closure phase matrices	22
3.2. Minimal complete sets	7	B.3. Log closure amplitude matrices	24
3.3. Redundant baselines	9	C. Worked examples of information content	25
4. Model fitting with unknown gains	10	C.1. Closure phase for $N = 3$ stations	26
4.1. Visibility covariance due to gain error	10	C.2. Closure phase for $N = 4$ stations	27
4.2. Model specifications	11	C.3. Closure amplitude for $N = 4$ stations	28
4.3. Phase modeling	12	C.4. Closure quantities for arbitrary $N$	28
4.4. Amplitude modeling	13	C.5. Explicit gain marginalization	30
4.5. Gain uncertainty modeling	14		

## 1. INTRODUCTION

Interferometric observations allow diffraction-limited resolution on angular scales that are inaccessible to single-element systems. However, interferometers have the limitation of only sparsely sampling information in the so-called visibility domain. While measured visibilities have simple and deterministic thermal noise, they also have complex systematic errors. These systematic errors manifest as variations in visibility amplitudes and phases on many timescales, representing limitations imposed by a broad range of sources including the constituent interferometer elements, reference frequencies, and atmosphere.

The dominant systematic errors are station-based effects, corresponding to multiplicative complex gain factors. In this case, “closure” quantities can be constructed, which are independent of the station-based systematic calibration errors. Specifically, closure phases consist of a directed sum of visibility phases around a closed triangle joining three stations (Jennison 1958; Rogers et al. 1974), while closure amplitudes are the quotient of two visibility products involving four stations (Twiss et al. 1960; Readhead et al. 1980). For an array with  $N$  stations, one can form  $\sim N^3$  closure phases and  $\sim N^4$  closure amplitudes from the original set of  $\sim N^2$  visibilities. However, there are at most  $(N-1)(N-2)/2$  degrees of freedom in the closure phases and  $N(N-3)/2$  degrees of freedom in the closure amplitudes. The necessary degeneracy between the full sets of closure quantities is captured by the structure of their covariance.

Closure quantities are useful for interferometric analysis, especially model fitting and imaging (e.g., Readhead & Wilkinson 1978; Chael et al. 2018), because they eliminate the need to model station gain systematics and their error budget can be determined from first principles. Yet, despite the fundamental importance of closure quantities for interferometry, there is widespread variation in the literature concerning their properties, best practices when utilizing closure quantities, their relationship with standard analyses such as self calibration, and the role of linearly independent sets of closure quantities (which are not necessarily statistically independent). Moreover, most analyses to date ignore the covariance between closure quantities, which can be significant, although covariance of closure phases has been studied in the optical interferometry community (e.g., Kulkarni et al. 1991; Martinache 2010; Ireland 2013).

Here, we provide a rigorous foundation for analysis using closure quantities, and we give procedures for selecting nonredundant sets of closure phases and amplitudes. We demonstrate that, when covariance is correctly accounted for, these nonredundant sets carry the full information of the complete sets of closure quantities. Moreover, in the limit of completely unconstrained station gains, we show that analysis of closure quantities is identical to analysis of complex

visibilities with gain marginalization. We also give procedures for selecting nonredundant sets that minimize covariance, and we demonstrate the effects of covariance among closure products using simulated data from simple models.

We begin, in Section 2, by discussing thermal and systematic errors in interferometric measurements, and we assess the conditions under which errors on closure quantities can be approximated as Gaussian. Next, in Section 3, we evaluate the covariance among closure quantities and give prescriptions for selecting nonredundant sets of closure quantities. Then, in Section 4, we apply our results to simple model fits using closure quantities and demonstrate the role of nonredundant sets and covariance among closure products. We summarize our results in Section 5. The notation used throughout the paper is described in Table 2.

## 2. CLOSURE QUANTITIES AND ERRORS

### 2.1. Interferometric visibility and gain

An interferometric array aims to measure the complex coherence function of the electric field, or *visibility*  $V_{ij} = E[E_i E_j^*]$  (represented here in the frequency domain, with  $E$  in units such that expectation value  $S_\nu \sim E[|E_i|^2]$  is the electromagnetic flux spectral density), from a distant source at two locations  $i$  and  $j$  in the plane of propagation.  $V_{ij}$  samples a Fourier component of the brightness distribution on the sky (via the van Cittert-Zernike theorem, van Cittert 1934; Zernike 1938; Thompson et al. 2017), with spatial frequency corresponding to the projected baseline length in units of observing wavelength. In the idealized case, the field is measured without any attenuation or propagation delays (e.g., through atmosphere). In practice, the measured complex signal  $v_i$  at an antenna  $i$  can be modeled as the idealized incident aligned electric field  $E_i$  subject to linear complex gain factor  $\gamma_i$ , plus additive zero-mean circularly-symmetric complex Gaussian noise  $n_i$

$$v_i = \gamma_i E_i + n_i. \quad (1)$$

In continuum-VLBI, the noise power typically exceeds signal power by a large factor:  $E[|n|^2] \gg E[|\gamma E|^2]$ . The gain for a particular antenna feed is a function of time and frequency  $\gamma = \gamma(t, f)$  and while a variety of simplifying assumptions and factorizations can be made, the gain is often not known *a priori* to a high degree of precision. Thus the fundamental observable is not source visibility  $V_{ij}$ , but cross-covariance  $r_{ij}$  between pairs of antennas:

$$r_{ij} = E[v_i v_j^*] = \gamma_i \gamma_j^* V_{ij}. \quad (2)$$

If the signals  $v_i$  and  $v_j$  are normalized by their noise power such that  $E[|n_i|^2] = 1$ ,  $r_{ij}$  is the correlation coefficient, and  $\text{SEFD}_i = 1/|\gamma_i|^2$  represents the *system-equivalent flux density* (noise power in units of flux above the atmosphere).

Relating the measured correlation coefficients  $r_{ij}$  to source visibilities  $V_{ij}$  is the process of *calibration* and may include estimating the magnitude of  $|\gamma_i|$  through the observation of bright flux calibrators, measuring differential phase  $\text{Arg}[\gamma_i \gamma_j^*]$  by observing phase calibrators with known structure, or by process of *self calibration* where the gains  $\gamma_i$  are solved simultaneously with unknown source model parameters. For a VLBI array at mm-wavelengths, calibration is made difficult by the strong and rapidly changing atmospheric effects and by the lack of bright compact calibration sources of known structure. Amplitude and phase gain systematics often dominate over the thermal (statistical) noise that arises from estimating  $r_{ij}$  over finite time and bandwidth.

## 2.2. Closure phase and closure amplitude

Closure quantities are special combinations of correlation measurements taken over closed loops in an antenna network. They are able to cancel out station-based gains  $\gamma_i$ , giving observables that depend only on intrinsic source parameters.

A *closure phase* is the sum of measured phases around a closed triangle of baselines,

$$\phi_{123} = \phi_{12} + \phi_{23} + \phi_{31}, \quad (3)$$

where  $\phi_{12}$  is the phase on baseline 1–2,

$$\phi_{12} = \text{Arg}[r_{12}]. \quad (4)$$

Written as the phase of the complex *bispectrum* (triple product)  $V_{123} = V_{12}V_{23}V_{31}$ , we see that a closure phase is independent of arbitrary phase gain  $\text{Arg}[\gamma_i]$ ,

$$\text{Arg}[r_{12}r_{23}r_{31}] = \text{Arg}[\gamma_1\gamma_2^*V_{12}\gamma_2\gamma_3^*V_{23}\gamma_3\gamma_1^*V_{31}] \quad (5)$$

$$= \text{Arg}[V_{12}V_{23}V_{31}], \quad (6)$$

since every gain term on the right-hand side is multiplied by its complex conjugate.

A set of correlation coefficients connecting four sites in a closed quadrangle can be used to calculate a *closure amplitude*,

$$\frac{|r_{12}||r_{34}|}{|r_{13}||r_{24}|} = \frac{|\gamma_1\gamma_2^*V_{12}||\gamma_3\gamma_4^*V_{34}|}{|\gamma_1\gamma_3^*V_{13}||\gamma_2\gamma_4^*V_{24}|} = \frac{|V_{12}||V_{34}|}{|V_{13}||V_{24}|}. \quad (7)$$

In this case we see that closure amplitude is independent of arbitrary amplitude gain  $|\gamma_i|$  since each station gain amplitude term appears in both the numerator and denominator.<sup>1</sup>

<sup>1</sup> This quadrangle can be easily cast as a complex closure quantity, but doing so provides no phase information beyond the set of complex bispectra. When taken over the four polarization feeds of a single baseline however, e.g.  $(V_{LR}V_{RL})/(V_{LL}V_{RR})$ , such a construction can provide some information about delay closure and/or polarization fraction.

By canceling station gains, the closure quantities are able to isolate measurement degrees of freedom which are independent from gains, and produce observables which are accurate to the thermal noise limit or to residual baseline errors (Massi et al. 1991) which are typically much smaller than the station errors. Thus they are particularly valuable when systematic gain uncertainty is much larger than statistical uncertainty. We will see in subsequent sections that the closure phases and closure amplitudes capture all the gain-invariant degrees of freedom from the baseline visibilities, at the cost of removing any prior information about the gains.

## 2.3. Statistical thermal noise

When estimated from actual data, the closure quantities and associated correlation coefficients from Equations 2–7 must be averaged over finite time and bandwidth in order to accumulate signal-to-noise (S/N). A measurement of  $r_{ij}$  taken over integration time  $\Delta t$  and bandwidth  $\Delta\nu$  averages  $\Delta t \Delta\nu$  independent complex samples (finite average denoted with  $\langle \rangle$ ), and includes contributions from both the source and the independent zero-mean (and normalized) thermal noise at each antenna,

$$r_{ij} = \check{r}_{ij} + \langle n_i n_j^* \rangle. \quad (8)$$

We have introduced a breve accent  $\check{r}_{ij} = \check{\gamma}_i \check{\gamma}_j^* \check{V}_{ij}$  to distinguish underlying (ground-truth) values from those that are subject to statistical or systematic errors.<sup>2</sup> The variance for one sample of correlated complex noise  $E[|n_i n_j^*|^2] = 1$ , and the variance in one component (real or imaginary) of the averaged complex noise correlation  $\langle n_i n_j^* \rangle$  is then,

$$\sigma_{r,ij}^2 = \frac{E[|\langle n_i n_j^* \rangle|^2]}{2} = \frac{1}{2\Delta t \Delta\nu}, \quad (9)$$

where the amount of time-frequency averaging to reduce  $\sigma_r^2$  is ultimately constrained by assumptions regarding station gain variability and source model variability.

The underlying signal-to-noise  $\check{\rho}$  of a correlation coefficient amplitude  $|\check{r}|$  under time-frequency averaging, and assuming negligible evolution of model visibility due to source structure or residual systematics, is

$$\check{\rho} = |\check{r}|/\sigma_r. \quad (10)$$

This is taken in the moderate-to-high  $\check{\rho}$  limit where it is meaningful to measure noise along just one of the complex components. A correlated flux density of 1 Jy with typical geometric mean SEFD of  $10^4$  Jy would give expected correlation coefficient of  $10^{-4}$  and a S/N of 4.5 over 1 GHz of bandwidth

<sup>2</sup> In principle the source contribution  $E[E_i E_j^*]$  is also subject to statistical fluctuations, i.e. the *self noise* of Kulkarni (1989), but these are strongly subdominant to uncertainties from thermal noise in the weak-signal limit  $E[|n|^2] \gg E[|\gamma E|^2]$  (Section 2.1).

in 1 s of integration time. At  $\check{\rho} < 1$ , the ability to measure correlation phase and amplitude degrades rapidly (Rogers et al. 1995), so that the minimum acceptable integration time is fundamentally limited by a combination of source strength, bandwidth, and collecting area.

At the same time, any uncompensated complex gain  $\check{\gamma}$  (from Equation 1, 2) must be stable over the averaging timescale to both ensure a meaningful measurement, and to avoid phase decoherence while vector averaging complex baseline visibility. At millimeter and submillimeter observing wavelengths, phase decoherence due to atmospheric turbulence occurs on timescales of seconds. The requirement that  $\check{\rho} > 1$  over an averaging time  $\Delta t$  and bandwidth  $\Delta \nu$  where gain variation remains negligible sets the observational constraints where the use of closure quantities is particularly effective. Gain variations over the frequency bandpass is generally a stable instrumental effect that can be well measured and calibrated out. For observations at high radio frequencies, rapid phase gain variability in time due to the atmosphere is a primary driver of efforts to expand the collecting area and instantaneous bandwidth of mm-VLBI arrays such as the EHT (Event Horizon Telescope Collaboration et al. 2019a,b), so that sufficient S/N can be accumulated within the correspondingly short averaging timescales.

In the following subsections, we discuss the consequences of low S/N on characterization of errors in phase and amplitude, and also the propagation of these errors across derived closure quantities. However, we do not explore optimal averaging strategies for the generation of closure phase and closure amplitudes. This would require assuming a prior model for gain variability. Rather we assume there exist some  $\Delta t$  and  $\Delta \nu$  such that  $\check{\rho} > 1$  is maintained on all baselines, and over which  $\check{\gamma}$  is reasonably stable.

#### 2.4. Non-Gaussian errors at low S/N

The observed correlation coefficients (Equations 8, 9) are subject to measurement noise that is complex and independent in real and imaginary components. While this implies that complex visibility is the natural measurement space for correlation observables, gain systematics are largely separable into amplitude factors (e.g. aperture efficiency) and phase factors (e.g. variable path delay), and this is reflected in the way closure phase and amplitude are formed.

The transformation from errors in real and imaginary coefficients to errors in amplitude and phase is only effectively linear for  $\check{\rho} \gg 1$ . A consequence is that the statistical error budget of closure quantities becomes progressively non-Gaussian as  $\check{\rho}$  becomes small. This is particularly severe for the case of reciprocal amplitude, which is a necessary component of closure amplitude (Equation 7). Heavy tails in the distribution for reciprocal amplitude are one motivation to

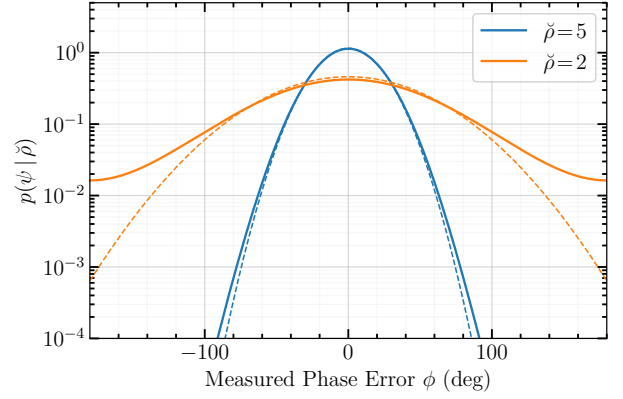


**Figure 1.** Distribution of closure phases versus Gaussian approximation from the high S/N theoretical limit (dashed lines). For each closure phase, all three baseline visibilities are drawn from a complex normal distribution with mean value  $\check{\rho}$  and unity variance in each complex component.

move to log closure amplitudes which place the numerator and denominator of a closure amplitude on equal footing.

We will primarily assume that measured amplitudes, log amplitudes, and phases for visibilities and for closure quantities can each be approximately, yet adequately characterized as a Gaussian random process with assumed model mean and variance. This is the case for  $\check{\rho} \gtrsim \text{few}$ , which is typically achieved in continuum radio interferometry through sufficient time-frequency averaging in the weak-signal limit. Examples of closure phase and closure amplitude distributions, along with corresponding high-S/N normal distribution approximations, are shown in Figures 1-2.

These ensemble distributions for measured phase and amplitude are exactly calculable for a given model  $\check{\rho}$ , even in the low  $\check{\rho}$  limit where the distributions become non-Gaussian. However, in practice the underlying intrinsic signal-to-noise  $\check{\rho}$  is generally not known, which means the distribution from which a single measured  $\rho$  is drawn is also not known precisely. Unless  $\check{\rho}$  is either assumed under a complete forward model (incorporating model visibility and all forward gains), or based on additional averaging beyond the single measurement of  $r$ , any estimate will be subject to thermal noise. In addition to a general mischaracterization of errors, this can also lead to a self-selection bias if realizations that are randomly low amplitude are assigned larger errors, or are preferentially flagged from the data.

An expanded description of phase and amplitude distributions is given in Appendix A. The distributions for phase, amplitude, and log amplitude can be reasonably approximated as Gaussian for  $\check{\rho}$  above 2–5. For log amplitude, a full characterization of the distribution under incoherent averaging of amplitudes is given in terms of moments. This is useful for estimating the a priori amplitude noise bias that becomes significant at low S/N.



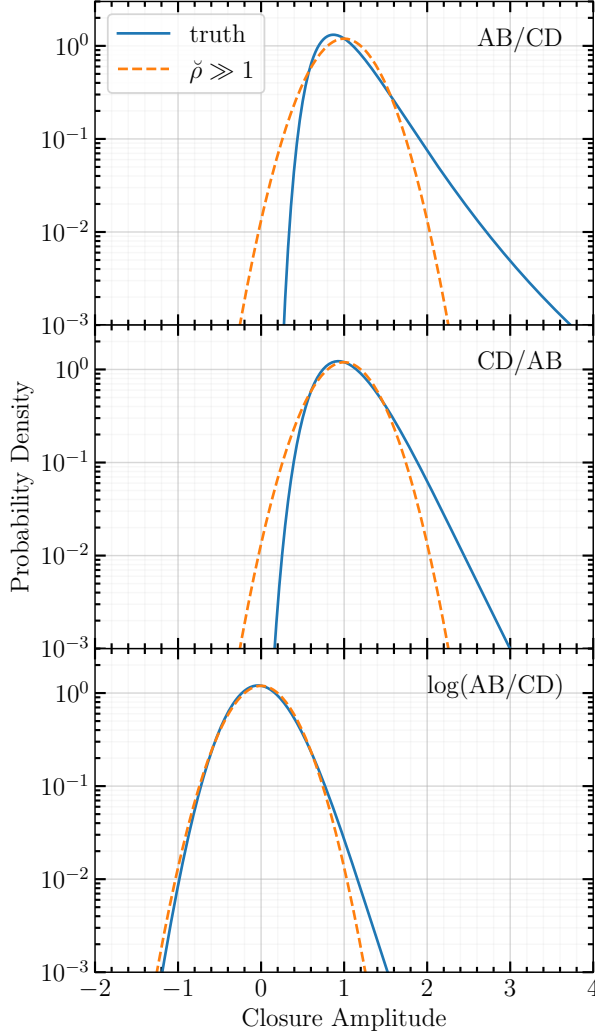


**Figure 2.** Distributions of closure amplitudes versus Gaussian approximations from the high-S/N theoretical limit. Baseline amplitudes A, B, C, D are drawn from a Rice distribution with noncentral amplitude 1 and  $\check{\rho}_A, \check{\rho}_B, \check{\rho}_C, \check{\rho}_D = (8, 8, 5, 5)$ . There are large tails in the standard closure amplitude ratio due to amplitudes in the denominator that approach zero (top panel). The tail is mitigated somewhat by placing the lower S/N measurements in the numerator (middle panel). However, using log closure amplitude provides a better behaved distribution overall (bottom panel).

### 3. INDEPENDENCE OF CLOSURE QUANTITIES

The  $\sim N^3$  possible closure phases and  $\sim N^4$  closure amplitudes are formed using the original  $\sim N^2$  baseline visibilities and become highly redundant at large  $N$ , where a much smaller subset of nonredundant quantities captures all source degrees of freedom (Readhead et al. 1980; Pearson & Readhead 1984). The codependence of redundant closure quantities and their initial construction from common baseline quantities leads to a general lack of statistical independence

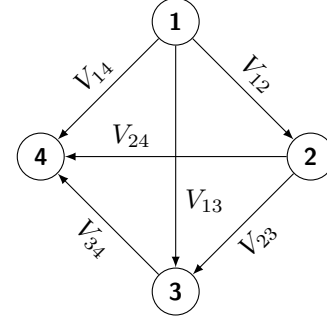


**Figure 3.** Network of four sites. There are 6 baselines, 3 nonredundant closure phases, and 2 nonredundant closure amplitudes.

in their residual thermal noise (Kulkarni 1989).<sup>3</sup> For closure phases and log closure amplitudes in the Gaussian limit,<sup>4</sup> the statistical dependence is fully characterized by a nonzero covariance.

In the following subsections, we detail the covariance structure for closure phases and log closure amplitudes, and we demonstrate the relationship of the covariance to the unique and statistically independent degrees of freedom present in the quantities. We then present strategies for the construction of nonredundant but complete sets of quantities, and discuss proper accounting of the number of gain-invariant degrees of freedom.

#### 3.1. Closure covariance due to thermal noise

Closure phases and log closure amplitudes are formed from sums and differences of shared baseline quantities, so that the closure quantities do not have independent noise. Under the approximation that baseline observables are Gaussian random variables, the joint distribution of  $T$  nonredundant closure phases  $\psi_{ijk}$ , for example, is characterized by a multivariate Gaussian distribution,

$$G(\psi; \hat{\psi}, \Sigma_\psi) = \frac{1}{\sqrt{(2\pi)^T \det(\Sigma_\psi)}} \exp \left[ -\frac{1}{2} \tilde{\psi}^\top \Sigma_\psi^{-1} \tilde{\psi} \right], \quad (11)$$

where residual closure phases  $\tilde{\psi} = \psi - \hat{\psi}$  are taken about model values  $\hat{\psi} = \{\hat{\psi}_{ijk}\}$  and have covariance matrix  $\Sigma_\psi$ .

<sup>3</sup> Although we focus here on the covariance of thermal noise, which is covariance in the residual measured quantities under a true source model, we note that the same relationships also hold for variations in structure closure phases and the analysis is relevant for isolating independent structural variability degrees of freedom that are measured across the array.

<sup>4</sup> The Gaussian limit is appropriate for  $S/N > \sim \text{few}$  (Section 2.4). Even at low  $S/N$ , closure quantities formed from a single set of baseline visibilities will be dependent by construction, but their statistical dependence cannot be characterized by a multivariate Gaussian due to nonlinear effects. However, in the special case of coherent ensemble averages over a very large number of closure quantities that have more than one low  $S/N$  baseline, the closure quantities become approximately statistically independent. This is often the case for bispectral averaging in optical interferometry where the atmospheric coherence time is extremely short (e.g., Kulkarni et al. 1991).

This corresponds to the likelihood of observing the residuals  $\tilde{\psi}$  under the model hypothesis.

For a collection of all baseline phases measured among four sites,  $\phi = \{\phi_{12}, \phi_{13}, \phi_{14}, \phi_{23}, \phi_{24}, \phi_{34}\}$  (Figure 3), the first three closure phases are,

$$\begin{aligned}\psi_{123} &= \phi_{12} + \phi_{23} - \phi_{13} \\ \psi_{124} &= \phi_{12} + \phi_{24} - \phi_{14} \\ \psi_{134} &= \phi_{13} + \phi_{34} - \phi_{14}\end{aligned}\quad (12)$$

The final closure phase is redundant with the other three,

$$\psi_{234} = \phi_{23} + \phi_{34} - \phi_{24} = \psi_{123} + \psi_{134} - \psi_{124}. \quad (13)$$

We can represent the generation of closure phases as a linear operator (closure phase design matrix  $\Psi$ ) applied to the baseline phases:  $\psi = \Psi\phi$ ,

$$\begin{pmatrix} \psi_{123} \\ \psi_{124} \\ \psi_{134} \end{pmatrix} = \begin{pmatrix} 1 & -1 & 0 & 1 & 0 & 0 \\ 1 & 0 & -1 & 0 & 1 & 0 \\ 0 & 1 & -1 & 0 & 0 & 1 \end{pmatrix} \begin{pmatrix} \phi_{12} \\ \phi_{13} \\ \phi_{14} \\ \phi_{23} \\ \phi_{24} \\ \phi_{34} \end{pmatrix}. \quad (14)$$

This closure phase design matrix is equivalent to the “phase closure operator” of Lannes (1990b) and the “phase compilation operator” of Lannes (1991).

The covariance matrix for the nonredundant set is  $\Sigma_\psi = \Psi \Sigma_\phi \Psi^\top$ , where  $\Sigma_\phi$  is the covariance of the measured baseline phases. In general  $\Sigma_\phi$  has a diagonal contribution from  $B$  independent baseline thermal noise contributions  $\mathbf{S} = \text{diag}(\sigma_{00}^2, \dots, \sigma_{BB}^2)$ , plus diagonal and off-diagonal contributions from common systematic gain errors  $\sigma_{\theta,i}^2$ . However the common gain errors are ultimately eliminated through the formation of closure quantities. Therefore,  $\Psi \Sigma_\phi \Psi^\top = \Psi \mathbf{S} \Psi^\top$ , and

$$\Sigma_\psi = \begin{pmatrix} \sigma_{12}^2 + \sigma_{23}^2 + \sigma_{13}^2 & \sigma_{12}^2 & -\sigma_{13}^2 \\ \sigma_{12}^2 & \sigma_{12}^2 + \sigma_{24}^2 + \sigma_{14}^2 & \sigma_{14}^2 \\ -\sigma_{13}^2 & \sigma_{14}^2 & \sigma_{13}^2 + \sigma_{34}^2 + \sigma_{14}^2 \end{pmatrix}. \quad (15)$$

The cross terms of  $\Sigma_\psi$  are nonzero and are based on the sign of the shared baseline components of each closure phase.

For the same network of four sites, the first two log-closure amplitudes are also based on sums and differences of log-baseline amplitudes  $\mathbf{a} = \{a_{12}, a_{13}, a_{14}, a_{23}, a_{24}, a_{34}\}$ ,

$$\begin{aligned}c_{1234} &= a_{12} + a_{34} - a_{13} - a_{24} \\ c_{1243} &= a_{12} + a_{34} - a_{14} - a_{23}\end{aligned}\quad (16)$$

with a third closure amplitude that is redundant,

$$c_{1342} = a_{13} + a_{24} - a_{14} - a_{23}. \quad (17)$$

By using log amplitude, the redundancy in closure amplitudes can be cast in terms of linear dependence, as is already the case for closure phases. Covariance terms are formed according to shared baselines, as was done for closure phases,

$$\Sigma_c = \begin{pmatrix} \sigma_{12}^2 + \sigma_{34}^2 + \sigma_{13}^2 + \sigma_{24}^2 & \sigma_{12}^2 + \sigma_{34}^2 \\ \sigma_{12}^2 + \sigma_{34}^2 & \sigma_{12}^2 + \sigma_{34}^2 + \sigma_{14}^2 + \sigma_{23}^2 \end{pmatrix} \quad (18)$$

The likelihood of observing a set of measured residual log closure amplitudes  $\tilde{\mathbf{c}} = \mathbf{c} - \hat{\mathbf{c}}$ , given measurements  $\mathbf{c}$  and model hypothesis  $\hat{\mathbf{c}}$ , parallels Equation 11 for closure phases,

$$\mathcal{L} = \frac{1}{\sqrt{(2\pi)^Q \det(\Sigma_c)}} \exp \left[ -\frac{1}{2} \tilde{\mathbf{c}}^\top \Sigma_c^{-1} \tilde{\mathbf{c}} \right]. \quad (19)$$

The covariance matrix  $\Sigma_c$  must be formed from a nonredundant set of  $Q \leq Q_{\text{minimal}}$  closure quantities – otherwise the matrix will be rank deficient and not invertible.  $Q_{\text{minimal}}$  is the minimum size set that captures all available degrees of freedom, as well as the largest nonredundant set that can be formed (this is demonstrated in Section 3.2). The value  $\tilde{\mathbf{c}}^\top \Sigma_c^{-1} \tilde{\mathbf{c}}$  will then follow a  $\chi^2$  distribution with  $Q$  degrees of freedom.

If we write the inverse covariance matrix as  $\Sigma_c^{-1} = \mathbf{U}^\top \Sigma_{c,\text{diag}}^{-1} \mathbf{U}$ , we see that matrix  $\mathbf{U}$  transforms a nonredundant set of  $Q_{\text{minimal}}$  closure quantities into a space of combinations of closure quantities with independent noise, and characterized by diagonal covariance matrix  $\Sigma_{c,\text{diag}}$ . When applied to closure phases, this generates the so-called “kernel phases”, first noted by Martinache (2010). The closure basis formed in this manner can be arbitrarily rotated by different choices of  $\mathbf{U}$ , but all rotations capture the same  $Q_{\text{minimal}}$  degrees of freedom. Additional redundant closure quantities to this set will be perfectly degenerate with linear combinations of the closure basis, and will not add additional information to the likelihood of a set of observations. Thus the calculation of  $\chi^2$  is unique and does not depend on the particular set of nonredundant closure quantities used (specific examples of this invariance are provided in Appendix C).

In terms of the closure (log amplitude) design matrix  $\mathbf{C}$ , the factorization can also be written,

$$\Sigma_c^{-1} = \Sigma_c^+ = (\mathbf{C}^+)^\top \mathbf{S}^{-1} \mathbf{C}^+ \quad (20)$$

where  $\mathbf{C}^+$  is the pseudo-inverse of  $\mathbf{C}$  and  $\mathbf{S}^{-1}$  is diagonal containing the reciprocal *baseline* thermal variances  $\sigma_{ij}^2$ .  $\mathbf{C}^+$  itself does not depend on the actual baseline noise, and can be readily computed via singular value decomposition (SVD). Redundant degrees of freedom will be reflected by singular values of zero, and can be avoided by first removing the redundant closure quantities by matrix reduction or explicit construction (Section 3.2). In that case the pseudo-inverse will be a true inverse. The advantage to inverting the design

matrix rather than the covariance matrix (as in Equation 11 or 19) is that the operation on the design matrix can be done once, and then applied to different baseline noise prescriptions with little computational cost.

### 3.2. Minimal complete sets

The total number,  $T$ , of triangles that can be constructed from a fully connected set of baselines across  $N$  sites is

$$T_{\text{all}} = \binom{N}{3} = \frac{N(N-1)(N-2)}{3!}, \quad (21)$$

while the number of closure phase degrees of freedom is only the total number of baseline phases ( $N(N-1)/2$ ) minus the number of degrees of freedom contained in site phase differences ( $N-1$ ). These degrees of freedom should be captured by a nonredundant subset of closure phases of size

$$T_{\text{minimal}} = \frac{(N-1)(N-2)}{2}. \quad (22)$$

For a large network, the set of all closure triangles will quickly outpace the number of independent measurements, resulting in a highly redundant set. One method for choosing a minimal set of closure triangles is given by Thompson et al. (2017) and shown in Figure 4. It involves selecting a single reference station and selecting the set of all triangles that contain it. Triangles that do not contain the reference station are formed as combinations of triangles from the minimal set.

We introduce a corresponding diagrammatic procedure for selecting a minimal set of closure amplitudes (Figure 5). The independent closure amplitudes are formed by arranging  $N$  sites on a ring, and selecting all pairs of two adjacent nonoverlapping sites. One closure amplitude is formed from each four-site arrangement (quadrangle) from the baselines which span the pair. Because the order of the pair does not matter, this results in the formation of

$$Q_{\text{minimal}} = \frac{N(N-3)}{2} \quad (23)$$

total closure amplitudes, equal to the  $N(N-1)/2$  baseline degrees of freedom minus the  $N$  unknown site gain factors. Combinations of closure amplitudes from the basis can be used to construct all remaining possible closure amplitudes, showing that the remaining closure amplitudes are redundant. Note that because adding a new station to the ring will necessarily break up one previous pair, the minimal set formed this way across  $N$  stations is not a proper subset of that formed across  $N+1$  stations. An alternative strategy for building the set of closure amplitudes in a staged matrix-driven approach is presented in Appendix B.3, and it is similar to the minimal closure quadrangle construction adopted in Chael et al. (2018).

In practice, the full set of  $N(N-1)/2$  baseline visibilities may not be available due to processing issues or by choice,

which complicates the generation of a minimal set of closure quantities. For closure phases, so long as a missing baseline does not include the reference station (Figure 4), the closure triangle containing the missing baseline can be excluded from the minimal set. For closure amplitudes, missing exterior baselines between adjacent sites along the ring (Figure 5) appear in only one of the closure amplitude basis quadrangles. Removing the quadrangle with the missing exterior baseline will correctly exclude all derivative closure amplitudes from the set. For more complicated baseline unavailability, a site-based procedure for forming nonredundant closure quantities may not work. One alternative method for extracting the unique degrees of freedom from a partially redundant set of closure quantities is through singular value decomposition (SVD) of the covariance matrix or design matrix (Equation 20, Figure 6). Alternatively a minimal set of the original closure quantities can be identified and extracted by matrix reduction of the design matrix.

An upper limit on the number  $n_\psi$  of different minimal closure phase subsets that exist for a fully-connected array with  $N$  stations is given by the binomial coefficient

$$n_\psi \leq \left( \frac{\text{size of maximal set}}{\text{size of minimal set}} \right) = \binom{\binom{N}{3}}{\binom{N-1}{2}}. \quad (24)$$

This expression yields only an upper limit because for a given maximal set and  $N > 4$ , some selections of subsets with size equal to that of the minimal set will contain redundant closure phases, and so will not themselves be valid minimal sets. An analogous upper limit holds for the number of nonredundant sets of closure amplitudes,

$$n_c \leq \binom{3\binom{N}{4}}{\frac{N(N-3)}{2}}. \quad (25)$$

Both  $n_\psi$  and  $n_c$  grow super-exponentially with  $N$  (see Table 1), and as the number of stations increases beyond a few it quickly becomes prohibitive to search through all possible nonredundant subsets for the one that minimizes covariance. The minimal-covariance subset for both closure phases and log closure amplitudes will generically depend on the specific baseline S/N distribution of the array, and we do not know of a general-purpose algorithm for selecting the optimal set. Instead, we consider rules of thumb for two limiting cases that approximate realistic array configurations: an array with uniform S/N on all baselines, and an array with S/N dominated by strong baselines to a single station or with other means to clearly identify weak baselines. We use the determinant of the correlation matrix,

$$\lambda \equiv \det(\boldsymbol{\varrho}), \quad (26)$$

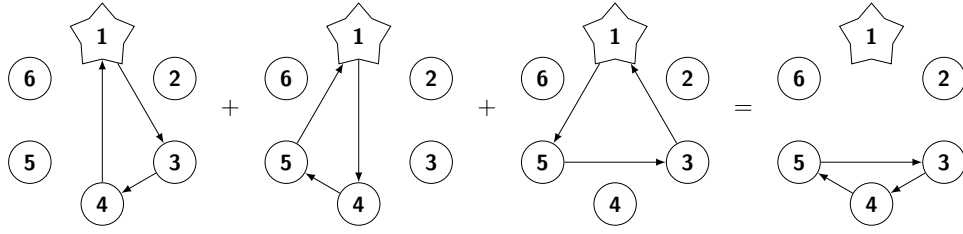


**Figure 4.** Construction of minimal set of closure phases. Site 1 is used as a reference, from which there are  $(N-1)(N-2)/2$  choices for the other two sites which build the set of all triangles containing site 1. Combinations of closure phases from this set can be used to form arbitrary triangles that do not contain the reference station, proving that the set is complete. This prescription is described in [Thompson et al. \(2017\)](#).

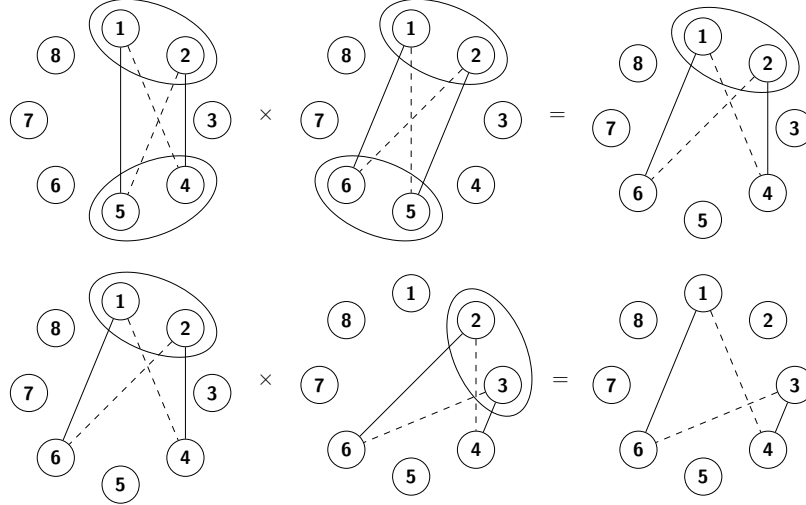


**Figure 5.** Construction of minimal set of closure amplitudes. We begin with the set of closure amplitudes defined by choosing all sets of two nonoverlapping pairs of adjacent sites and forming one closure amplitude from each collection of four sites according to the baselines shown on the top left. Solid and dashed lines determine which baselines go in the numerator and denominator of the closure amplitude. Since there are  $N$  choices for the placement of the first adjacent pair, and  $N-3$  choices for the placement of the second pair, there are  $N(N-3)/2$  nonredundant closure amplitudes formed. By multiplying closure amplitudes from our set, we can construct arbitrary closure amplitudes containing nonadjacent sites. The set is therefore complete.

to quantify the degree of independence for any specific choice of minimal subset, where the elements of  $\mathbf{g}$  are related to the elements of the covariance matrix  $\Sigma$  by

$$\varrho_{ij} = \frac{\Sigma_{ij}}{\sqrt{\Sigma_{ii}\Sigma_{jj}}}. \quad (27)$$

The value of  $\lambda$  varies between zero and one, with  $\lambda = 1$  corresponding to no correlation and  $\lambda = 0$  corresponding to complete correlation.

For an array with uniform S/N on all baselines (e.g., a homogeneous array observing a point source), the covariance is minimized (i.e.,  $\lambda$  is maximized) when all stations are represented as nearly equally as possible<sup>5</sup> in the minimal set of

either closure phases or log closure amplitudes. For example, an array with  $N = 6$  stations has a minimal closure phase set size of 10, but of the  $n_\psi = 46620$  different choices of minimal set only 12 equally represent all baselines.<sup>6</sup> Similarly, an array with  $N = 5$  stations has a minimal log closure amplitude set size of 5, but only 6 out of  $n_c = 1518$  minimal sets equally represent all baselines.<sup>7</sup>

For an array with high S/N on baselines to only one station (e.g., a heterogeneous array containing one highly sensitive station), the closure phase covariance is minimized when the minimal set is constructed using only triangles containing the reference station ([Chael et al. 2018](#)); that is, using the minimal set construction algorithm described earlier in this section produces an optimal set when the reference station dominates the array sensitivity. This is because weak baselines

<sup>5</sup> Note that it is almost never the case that strictly equal representation of all baselines is possible; for closure phases, only the  $N = 3$  and  $N = 6$  arrays can achieve perfect balance (with each baseline represented exactly once or twice, respectively), while log closure amplitudes are limited to only the  $N = 5$  array (with each baseline represented exactly twice) and  $N = 9$  array (with each baseline represented exactly three times).

<sup>6</sup> An example such set is  $\{\psi_{123}, \psi_{124}, \psi_{135}, \psi_{146}, \psi_{156}, \psi_{236}, \psi_{245}, \psi_{256}, \psi_{345}, \psi_{346}\}$ .

<sup>7</sup> An example such set is  $\{c_{1234}, c_{1245}, c_{1352}, c_{1453}, c_{2345}\}$ .



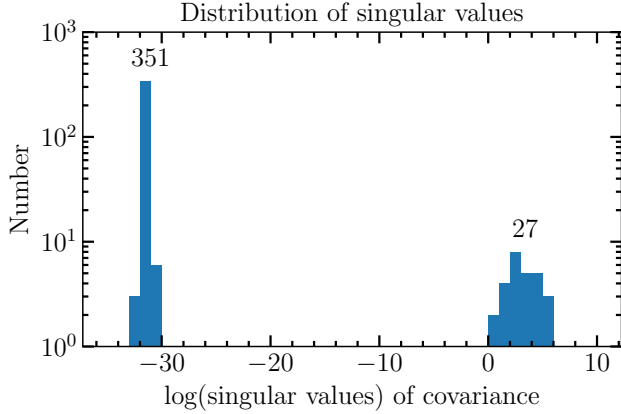


**Figure 6.** Singular value decomposition of the covariance matrix formed from a full set of 378 closure amplitudes over 9 sites. The baseline noise prescription is random. There are 27 nonzero singular values corresponding to the  $9 \times (9 - 3)/2 = 27$  independent degrees of freedom represented in the closure amplitudes. SVD is particularly useful in situations of arbitrary missing baselines which complicates the direct generation of a minimal set of closure quantities.

**Table 1.** Unique minimal sets

$N$	$n_b$	$n_c$
3	1	...
4	4	3
5	125	1518
6	46620	351117922

NOTE—The number of unique minimal sets of closure phases and log closure amplitudes for small arrays.

between two non-reference stations are then used only once in the construction. For log closure amplitudes, placing the lowest S/N baselines on the ring as adjacent sites (as in Figure 5) accomplishes the same goal; the weakest baselines are used only once in the minimal set and thus do not contribute to the overall covariance.

### 3.3. Redundant baselines

Some interferometric arrays have multiple baselines that are effectively redundant (dense arrays are often designed with this redundancy, to aid calibration). For instance, a common case in VLBI is to have multiple sites that can effectively be considered colocated. For example, the CSO, JCMT, and SMA are all on Mauna Kea and have participated in EHT experiments. Likewise, the APEX telescope is located within a few kilometers of the ALMA phased array center. Baselines to these redundant sites sample the same visibility and

source structure, and they can be combined to reduce thermal noise and to improve calibration. For example, the addition of ALMA to the EHT including APEX does not provide new baselines. However, it significantly reduces the thermal noise of baselines to Chile.

We have so far focused on the unique statistical degrees of freedom contained in the closure quantities, which does not depend on array geometry. Baseline redundancy does have a dramatic effect, however, on the unique source structure degrees of freedom measured by the array. For example the addition of colocated sites to a VLBI network does not sample new nontrivial source information via closure phases even as the statistical degrees of freedom grow according to Equation 23, but it does increase the amount of source information measured via closure amplitudes. In the limit where every site has a redundant partner, all source visibility amplitude information is sampled via closure amplitudes apart from a single unknown degree of freedom for the total flux density.

To assess the independent degrees of freedom for an array with baseline redundancy, we introduce a redundancy matrix  $\mathbf{R}$  of dimensions  $B_{\text{NR}} \times B$  which links multiple measurements from redundant baselines into a single degree of freedom, such that  $B_{\text{NR}} \leq B$  is the number of nonredundant geometric baselines that sample unique source structure. For each row corresponding to a unique geometric baseline,  $\mathbf{R}$  contains a 1 in each column for each matching station pair. If there are no redundant baselines,  $\mathbf{R}$  is the identity matrix. For the four site network in Figure 3, if stations 1 and 2 are taken to be colocated, then of the six measured baselines  $\{V_{12}, V_{13}, V_{14}, V_{23}, V_{24}, V_{34}\}$ ,  $V_{13}$  &  $V_{23}$  sample the same geometric baseline, as do  $V_{14}$  &  $V_{24}$ , so that

$$\mathbf{R} = \begin{pmatrix} 1 & 0 & 0 & 0 & 0 & 0 \\ 0 & 1 & 0 & 1 & 0 & 0 \\ 0 & 0 & 1 & 0 & 1 & 0 \\ 0 & 0 & 0 & 0 & 0 & 1 \end{pmatrix} \quad (28)$$

with the “zero baseline”  $V_{12}$  serving as one of the four unique geometric baselines.

The number of unique source degrees of freedom captured by closure quantities is found by taking rank of the compound design matrix which converts nonredundant amplitudes to closure quantities. For the previous four station example with one colocated pair, this gives  $\text{rank}(\Psi \mathbf{R}^T) = 2$  gain-independent phase structure degrees of freedom, and  $\text{rank}(\mathbf{C} \mathbf{R}^T) = 1$  gain-independent amplitude structure degrees

of freedom.<sup>8</sup> A four site array arranged in a square satisfies different constraints with  $V_{12} \sim V_{34}$  and  $V_{14} \sim V_{23}$ . While there are still four unique geometric baselines, there are now  $\text{rank}(\Psi \mathbf{R}^\top) = 3$  structure closure phases and  $\text{rank}(\mathbf{C} \mathbf{R}^\top) = 2$  structure closure amplitudes, both equal to the corresponding number of linearly independent closure quantities.

The analysis indicates that by judicious use of redundancy, an interferometric array can reduce the overall complexity of the measurements (with  $\text{rank}(\mathbf{R})$  as an indication of complexity) while not sacrificing measured gain-independent structure degrees of freedom. For example,  $\text{rank}(\mathbf{R}) - \text{rank}(\mathbf{C} \mathbf{R}^\top)$  can be taken as an indication of the number of “amplitude gains” which remain unconstrained. However, as some level of a priori gain information is often possible, a sparse array which samples the maximum number of unique geometric baselines is likely preferable over one that utilizes geometric redundancy for most situations. Colocated sites in particular can cause a significant loss in measured information. However they do provide a link to zero baseline quantities (such as total flux), which are generally known a priori and thus inform model independent calibration (Blackburn et al. 2019).

#### 4. MODEL FITTING WITH UNKNOWN GAINS

In this section we apply the closure construction procedures detailed in the appendices to perform a series of simple model fits to different simulated data products generated from the same underlying truth image. The goal of these tests is to demonstrate that the same model parameter posteriors can be recovered using different representations of the data products, so long as covariances between measurements are properly accounted for.

##### 4.1. Visibility covariance due to gain error

To connect model fitting to closure quantities with model fitting to baseline visibilities, we first introduce a parallel construction (to Section 3.1) for the covariance in visibility measurements under the presence of uncertainty in station gain. In both cases we characterize the covariance in a residual quantity ( $\tilde{\psi}$  or  $\tilde{c}$  for closure quantities,  $\tilde{\phi}$  or  $\tilde{a}$  for visibilities – see Table 2). However, while the covariance for residual closure quantities is due to thermal error on shared baselines, the baseline thermal noise is independent for visibility quantities in the weak source limit, and the covariance is due to systematic error in model gain over shared stations. A vis-

ibility measurement  $V_{ij}$  contains contributions from both the source and from the station gains,

$$V_{ij} = \gamma_i \gamma_j^* r_{ij}. \quad (29)$$

The multiplicative complex gains manifest as additive terms modifying the visibility phases and log visibility amplitudes,

$$\phi_{ij} = \check{\phi}_{ij} + \theta_i - \theta_j, \quad (30a)$$

$$a_{ij} = \check{a}_{ij} + g_i + g_j, \quad (30b)$$

where the sign differences in the second gain terms arise because complex conjugation negates phases but leaves amplitudes unchanged.

More generally, we can express the gain contributions to a collection of visibility phases or log visibility amplitudes in terms of design matrices  $\Phi$  or  $\mathbf{A}$  operating on the vector of gain phases or log gain amplitudes,

$$\phi = \check{\phi} + \Phi \theta, \quad (31a)$$

$$\mathbf{a} = \check{\mathbf{a}} + \mathbf{A} \mathbf{g}. \quad (31b)$$

For example, the visibility phases measured on the baselines in Figure 3 can be expressed using

$$\begin{pmatrix} \phi_{12} \\ \phi_{13} \\ \phi_{14} \\ \phi_{23} \\ \phi_{24} \\ \phi_{34} \end{pmatrix} = \begin{pmatrix} \check{\phi}_{12} \\ \check{\phi}_{13} \\ \check{\phi}_{14} \\ \check{\phi}_{23} \\ \check{\phi}_{24} \\ \check{\phi}_{34} \end{pmatrix} + \begin{pmatrix} 1 & -1 & 0 & 0 \\ 1 & 0 & -1 & 0 \\ 1 & 0 & 0 & -1 \\ 0 & 1 & -1 & 0 \\ 0 & 1 & 0 & -1 \\ 0 & 0 & 1 & -1 \end{pmatrix} \begin{pmatrix} \theta_1 \\ \theta_2 \\ \theta_3 \\ \theta_4 \end{pmatrix}, \quad (32)$$

while the log visibility amplitudes can be similarly expressed using

$$\begin{pmatrix} a_{12} \\ a_{13} \\ a_{14} \\ a_{23} \\ a_{24} \\ a_{34} \end{pmatrix} = \begin{pmatrix} \check{a}_{12} \\ \check{a}_{13} \\ \check{a}_{14} \\ \check{a}_{23} \\ \check{a}_{24} \\ \check{a}_{34} \end{pmatrix} + \begin{pmatrix} 1 & 1 & 0 & 0 \\ 1 & 0 & 1 & 0 \\ 1 & 0 & 0 & 1 \\ 0 & 1 & 1 & 0 \\ 0 & 1 & 0 & 1 \\ 0 & 0 & 1 & 1 \end{pmatrix} \begin{pmatrix} g_1 \\ g_2 \\ g_3 \\ g_4 \end{pmatrix}. \quad (33)$$

The visibility phase design matrix is equivalent to the “phase aberration operator” of Lannes (1990b), while the log visibility amplitude design matrix matches the “amplitude aberration operator” of Lannes (1990a, 1991).

This additivity makes it convenient to model the gain phases and log gain amplitudes as Gaussian-distributed, so that their variances simply add to those of the corresponding visibility quantities. The baseline-based thermal variances

<sup>8</sup> The construction does not impose a trivial phase for the zero baseline, but it can be assumed by explicitly removing the corresponding row from  $\mathbf{R}$ . Doing so leaves 1 remaining phase structure degree of freedom corresponding to the single open triangle. There is also a trivial closure amplitude for the case of a colocated pair of sites where each baseline in the numerator has a matching baseline in the denominator with the same amplitude. In this case the trivial behavior is already fully captured by the closure amplitude design matrix  $\mathbf{C}$  and does not need to be taken *a priori*.

are uncorrelated across baselines, and in the absence of gains would fully describe the visibility covariances via the diagonal matrices  $\mathbf{S}_\phi$  for visibility phases and  $\mathbf{S}_a$  for log visibility amplitudes (see Table 3 and Table 4 in Appendix B.1). The station-based gain variances do drive covariances in the visibility residuals for baselines that share a station, with the design matrices serving to map stations to baselines. The covariance matrices are then constructed as the sum of the baseline-based and station-based contributions,

$$\Sigma_\phi = \mathbf{S}_\phi + \Phi \Sigma_\theta \Phi^\top, \quad (34a)$$

$$\Sigma_a = \mathbf{S}_a + \mathbf{A} \Sigma_g \mathbf{A}^\top, \quad (34b)$$

with the off-diagonal elements consisting of only station-based terms while the diagonal elements combine both station-based and baseline-based terms. The covariance matrix corresponding to the visibility phases in Equation 32 is given by

$$\Sigma_\phi = \begin{pmatrix} \sigma_{12}^2 + \sigma_{\theta,1}^2 + \sigma_{\theta,2}^2 & \sigma_{\theta,1}^2 & \dots & 0 \\ \sigma_{\theta,1}^2 & \sigma_{13}^2 + \sigma_{\theta,1}^2 + \sigma_{\theta,3}^2 & \dots & -\sigma_{\theta,3}^2 \\ \sigma_{\theta,1}^2 & \sigma_{\theta,1}^2 & \dots & 0 \\ -\sigma_{\theta,2}^2 & \sigma_{\theta,3}^2 & \dots & -\sigma_{\theta,3}^2 \\ -\sigma_{\theta,2}^2 & 0 & \dots & 0 \\ 0 & -\sigma_{\theta,3}^2 & \dots & \sigma_{34}^2 + \sigma_{\theta,3}^2 + \sigma_{\theta,4}^2 \end{pmatrix}, \quad (35)$$

while the covariance matrix corresponding to the log visibility amplitudes in Equation 33 is structurally identical except for the off-diagonal term signs,

$$\Sigma_a = \begin{pmatrix} \sigma_{12}^2 + \sigma_{g,1}^2 + \sigma_{g,2}^2 & \sigma_{g,1}^2 & \dots & 0 \\ \sigma_{g,1}^2 & \sigma_{13}^2 + \sigma_{g,1}^2 + \sigma_{g,3}^2 & \dots & \sigma_{g,3}^2 \\ \sigma_{g,1}^2 & \sigma_{g,1}^2 & \dots & 0 \\ \sigma_{g,2}^2 & \sigma_{g,3}^2 & \dots & \sigma_{g,3}^2 \\ \sigma_{g,2}^2 & 0 & \dots & 0 \\ 0 & \sigma_{g,3}^2 & \dots & \sigma_{34}^2 + \sigma_{g,3}^2 + \sigma_{g,4}^2 \end{pmatrix}. \quad (36)$$

The likelihood of observing a collection of  $B = N(N-1)/2$  residual visibility phases under a given source and gain model is then,

$$\mathcal{L} = \frac{1}{\sqrt{(2\pi)^B \det(\Sigma_\phi)}} \exp \left[ -\frac{1}{2} \tilde{\phi}^\top \Sigma_\phi^{-1} \tilde{\phi} \right], \quad (37)$$

with a similar construction for log visibility amplitudes  $\mathbf{a}$ . This likelihood reduces to the simple case of statistically independent measured visibilities in the limit of zero systematic gain error (i.e., perfectly calibrated data).

#### 4.2. Model specifications

We consider the simple geometric truth image shown in the left panel of Figure 7. This image is constructed from the sum of two elliptical Gaussian components that are symmetrically positioned about the origin with a mutual separation of  $\xi = 50 \mu\text{as}$  and a position angle of  $\eta = 75$  degrees East of North. Both components have major and minor axis Gaussian  $\sigma$ -values of  $9 \mu\text{as}$  and  $6 \mu\text{as}$ , respectively, and each has a flux density of  $0.5 \text{ Jy}$ . The major axis of the eastern component is oriented at  $30$  degrees East of North, while the western component has a  $-30$  degree orientation. These specific choices of parameter values are largely arbitrary, and they serve primarily to give the image sufficient asymmetry to produce nontrivial visibility phases and sufficient compactness to produce nonzero visibility amplitudes.

To produce synthetic visibility data, we sample the Fourier transform of the truth image at discrete locations in  $(u, v)$  space. We consider two sets of  $(u, v)$  coverage, corresponding to (1) a single snapshot from an  $N = 8$  station array with mutual visibility to all stations and (2) an  $N = 5$  station subset of that array. Both sets of coverage are shown in the right panel of Figure 7. Visibility amplitudes and phases are given by the magnitude and argument of the complex visibilities from each  $(u, v)$  point. The visibilities are then multiplied by their associated station gains, which are simulated as complex Gaussian-distributed random variables with unit mean and standard deviation of  $0.1$  along each dimension. Closure phases are constructed from the visibility phases using Equation C60, and log closure amplitudes are constructed from the visibility amplitudes using Equation C67.

We model the data as the sum of two elliptical Gaussians, with all parameters except for  $\xi$  and  $\eta$  held fixed at their corresponding truth values. By restricting the model to this two-dimensional subspace of its natural 12-dimensional parameter space, we simplify the fitting process while retaining enough model complexity to provide nontrivial parameter correlations. We perform parameter estimation using Gaussian likelihoods analogous to Equation 37 for all data products. Unless otherwise specified, we apply uniform priors on the range  $[40, 60] \mu\text{as}$  for  $\xi$  and  $[0, 180]$  degrees for  $\eta$ ; when fitting gains, our “maximally uninformative” priors are log-uniform on the range  $[10^{-5}, 10^5]$  for all gain amplitudes and uniform priors on the range  $[0, 360]$  degrees for all gain phases. We use the Python nested sampling code *dynesty*<sup>9</sup> (Speagle 2019) to produce parameter posteriors for all model fits.

<sup>9</sup> <https://github.com/joshspeagle/dynesty>

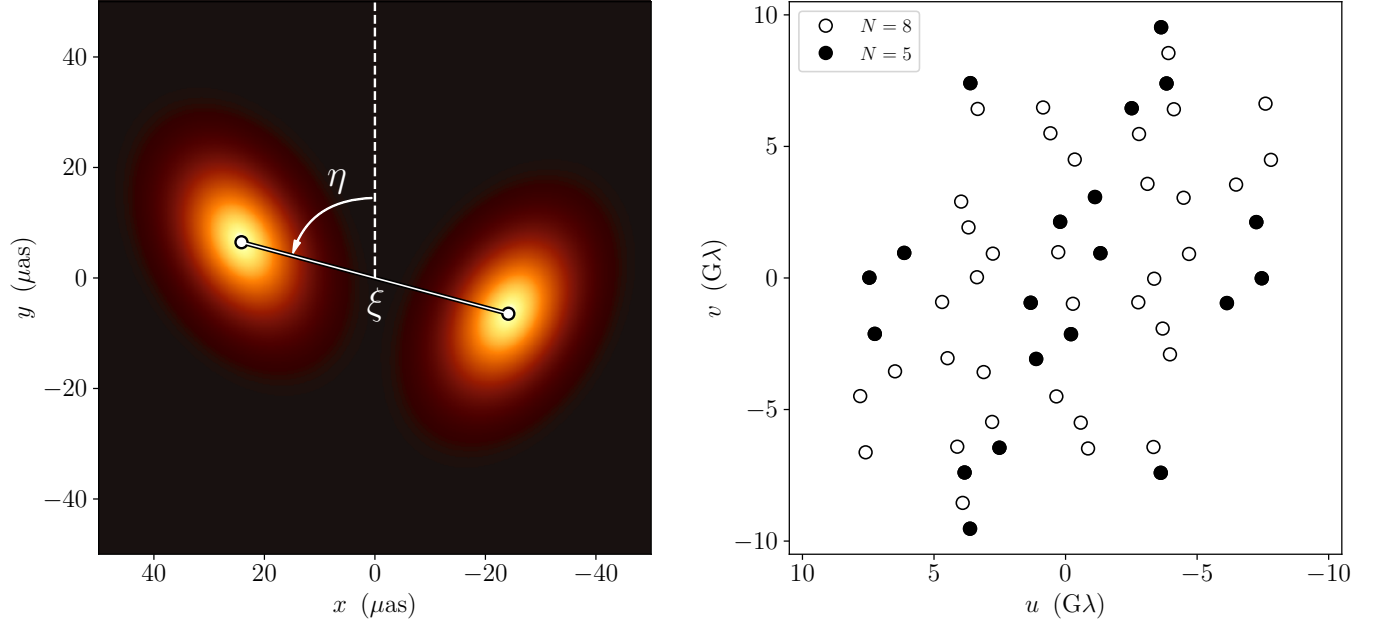


**Figure 7.** Truth image (left) and  $(u, v)$  coverage (right) for the model considered in Section 4. The truth image contains two elliptical Gaussian components with an arbitrary but specific separation and relative orientation angle; all defining parameters are fixed during model-fitting except for the component separation  $\xi$  and position angle  $\eta$ . The  $(u, v)$  coverage represents that from a single simultaneous observation with mutual visibility to all stations; we consider both an array with  $N = 8$  stations of equal sensitivity as well as a subset containing only  $N = 5$ . The resulting baseline S/N measurements span a factor of  $\sim 20$ .

#### 4.3. Phase modeling

We fit the model to synthetic phase data represented in a variety of ways, starting with visibility phases under the assumption that the gain phases are perfectly known (or equivalently, that they are perfectly calibrated). The likelihood function for this representation is given by Equation 37, and because the gain phases are known the visibility phase covariance matrix is diagonal. Figure 8 shows the two-dimensional  $(\xi, \eta)$  posteriors for such fits to the  $N = 8$  array and  $N = 5$  array data in black contours.

We also fit the model to visibility phase data without assuming any *a priori* knowledge of the gain phases. The likelihood function remains Equation 37, but in this case the covariance matrix is no longer diagonal. The gray contours in Figure 8 show the corresponding joint posteriors for  $(\xi, \eta)$ , which exhibit the expected loss of constraining power compared to the posteriors derived from calibrated visibility phases. We can see that this loss becomes less severe as the number of stations increases, a consequence of the fact that the fraction of the visibility phase information required to constrain the gain phases decreases as  $2/N$ .

The other phase data representations we consider are closure phases. For a minimal subset of closure phases described by covariance matrix  $\Sigma_\psi$  (see Appendix B.2), the likelihood function is given by Equation 11. Posteriors derived from this likelihood are shown as red dashed contours in Figure 8. Within the  $\sim 1\%$  numerical sampling uncertain-

ties of our posterior contours, the closure phases provide parameter constraints that are identical to those imposed by the uncalibrated visibility phases.

We also consider two alternative treatments of the closure phases that attempt to avoid accounting for covariances, and we show here that these efforts fail. In the first such treatment, we use a minimal closure phase subset but assume all measurements are independent. This assumption amounts to using only the diagonal elements of  $\Sigma_\psi$  (i.e., all off-diagonal elements are set to zero), and the likelihood function remains Equation 11. The red and blue contours in the left panel of Figure 9 show posteriors derived under this assumption, for two different choices of minimal closure phase subset constructed by ordering the stations from lowest to highest (red) and highest to lowest (light blue) mean baseline S/N. We can see that these contours systematically deviate from the visibility phase contour. In the second treatment we use the maximal (redundant) set of closure phases (see Appendix B.2), but we retain the assumption that all measurements are independent. The likelihood is then simply the product of the individual measurement likelihoods taken over all closure phases in the maximal set. The dotted black contour in the left panel of Figure 9 represents the resulting posterior after scaling the individual measurement variances by

$$R_\psi = \binom{N}{3} / \binom{N-1}{2} = \frac{N}{3}, \quad (38)$$

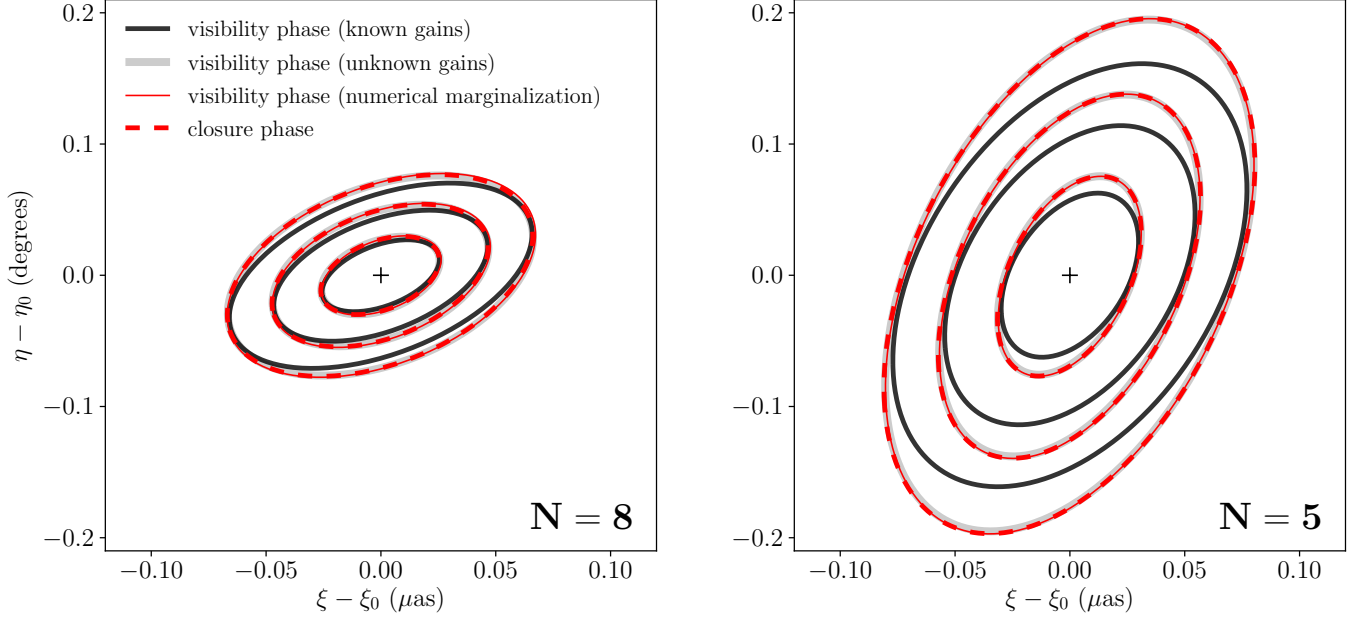


**Figure 8.** Joint posterior distributions for residual separation ( $\xi - \xi_0$ ) and position angle ( $\eta - \eta_0$ ) when fitting the model described in Section 4 to visibility phases with perfectly known gain phases (black contours), visibility phases with completely unknown gain phases (gray contours), and closure phases with covariant structure accounted for (red dashed contours). We also show the results from numerically marginalizing over the gains (thin black contours), which match the covariant treatment as expected (see Appendix C.5). The model is fitted to the 8-station array data on the left and to the 5-station array data on the right; we can see that the relative loss of information when going from perfectly calibrated phases to closure phases increases for smaller arrays. In both cases the closure phase fits accurately recover the posteriors derived from visibility phase fits, within sampling uncertainties. Contours enclose 50%, 90%, and 99% of the posterior probability.

which is a redundancy factor that accounts for the fact that the maximal set contains an increased number of measurements without a corresponding increase in the number of degrees of freedom. Even after accounting for this redundancy, however, we see a similar systematic discrepancy in the posterior relative to those derived from the visibility phases. Note that for the unusual case of equal S/N on all baselines, this redundancy factor scaling does produce the correct likelihood (see Appendix C).

#### 4.4. Amplitude modeling

We perform a set of model fits that are analogous to those presented in Section 4.3, but for visibility amplitudes and log closure amplitudes rather than visibility phases and closure phases. The black contours in Figure 10 show the  $(\xi, \eta)$  posteriors for fits to the  $N = 8$  and  $N = 5$  array visibility amplitude data, using a likelihood analogous to Equation 37 under the assumption of perfectly calibrated gain amplitudes. The gray contours show fits to visibility amplitudes using the same likelihood but assuming no knowledge of the gain amplitudes. We again see the relative loss of information increasing as the number of stations decreases, becoming particularly severe for the case of  $N = 5$  (in which there are only 3 degrees of freedom remaining in the data to constrain the model, compared to 8 degrees of freedom when the gain amplitudes are calibrated).

We compare the visibility amplitude results to those obtained from fitting to log closure amplitudes. For a minimal subset of log closure amplitudes described by a covariance matrix  $\Sigma_c$  (see Appendix B.3), the likelihood function is given by Equation 19. The posteriors derived using this likelihood expression are plotted in Figure 10 as red dashed contours. As with the closure phases, we find that the log closure amplitudes provide constraints that are identical to those provided by the uncalibrated visibility amplitudes.

In the right panel of Figure 9, we again compare the posteriors obtained using (1) a minimal set of log closure amplitudes without accounting for covariance, and (2) a maximal set of log closure amplitudes. In both cases the likelihood function is the product of the individual measurement likelihoods, where the product is taken over all log closure amplitudes in the minimal or maximal set, as appropriate. We again consider two choices of minimal subset, constructed via the same station ordering scheme used in Section 4.3. For the posteriors derived from the maximal set, shown using a dotted black contour in the right panel of Figure 9, we have scaled the measurement variances by the redundancy factor

$$R_A = 3 \binom{N}{4} / \left( \frac{N(N-3)}{2} \right) = \frac{(N-1)(N-2)}{4}. \quad (39)$$



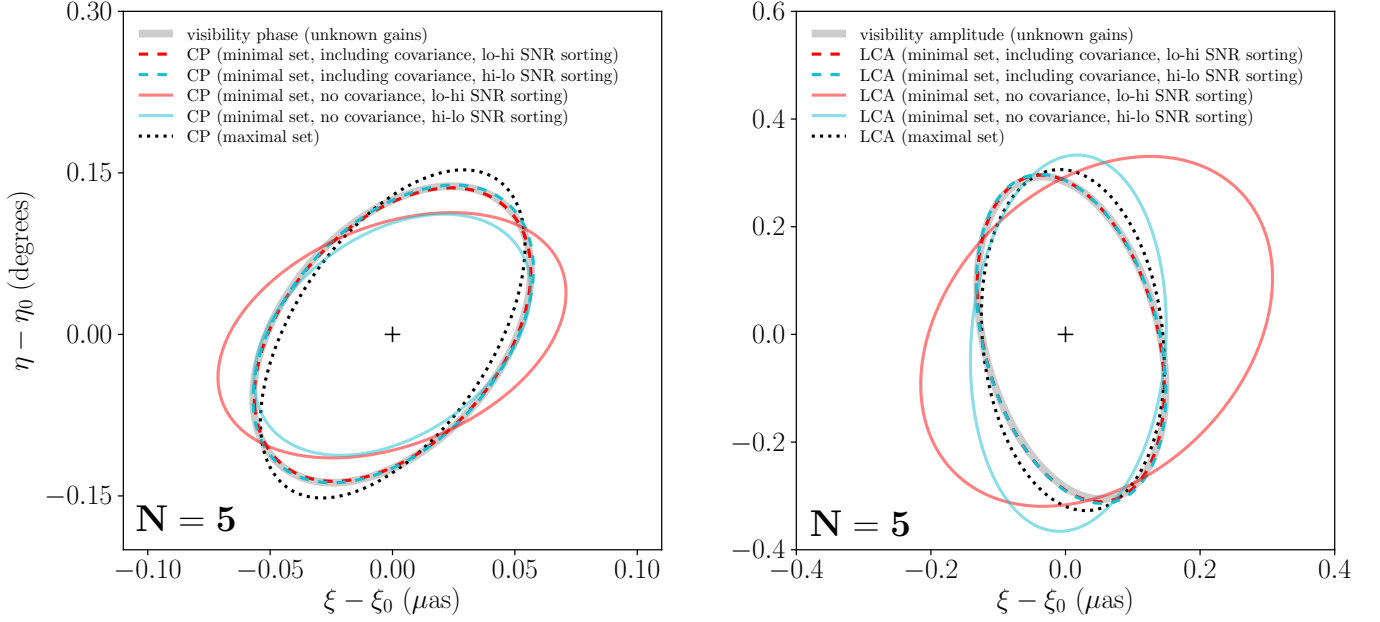


**Figure 9.** *Left:* Same as left panel of Figure 8, but showing additional posteriors as calculated for different closure phase (CP) likelihood constructions. The posteriors obtained when including closure phase covariance (dashed contours) demonstrate the most consistency with the uncalibrated visibility phase posterior (yellow contour). The blue and red contours show posteriors constructed from fitting a minimal closure phase set but ignoring covariance, while the dotted black contour shows the posterior constructed from a maximal (redundant) set of closure phases that has been corrected for redundancy factor (see Equation 38). All three show artificial distortions in the confidence regions. *Right:* Analogous to the left panel, but for the log closure amplitudes (LCA) rather than closure phases; the redundancy factor for the maximal set is given by Equation 39. The contours in both panels enclose 90% of the posterior probability.

Regardless of the redundancy correction, we find in both cases that the posterior distributions do not match those expected from fits to the visibility amplitudes.

#### 4.5. Gain uncertainty modeling

We have shown that our level of knowledge about the gains dictates how much source information the closure quantities contain relative to the visibility quantities. For perfectly known (or, equivalently, perfectly calibrated) gains, the visibility quantities provide more information about the source than the closure quantities; for small arrays, this difference may be quite large (see, e.g., Figure 10). When the gains are completely unknown (or, equivalently, when the gains must be fully determined along with the source information), both the visibility and closure quantities contain identical source information. We now explore the case of partially-known gains.

We quantify how well we know the gains by comparing our gain uncertainty,  $\sigma_i$ , to the uncertainties in the data (i.e., in the visibilities),  $\sigma_{ij}$ , using

$$\varepsilon \equiv \frac{\langle \sigma_{ij} \rangle}{\langle \sigma_i \rangle}, \quad (40)$$

where  $\langle \rangle$  denotes a sample average; the averages are taken over all stations and all baselines for the gain uncertainties and visibility uncertainties, respectively. The quantity

$\varepsilon$  tracks our knowledge of the gains;  $\varepsilon \rightarrow 0$  when we have no information about the gains, and  $\varepsilon \rightarrow \infty$  when the gains are perfectly calibrated. Note that both  $\sigma_i$  and  $\sigma_{ij}$  refer to logarithmic uncertainties when considering amplitude data products, meaning that  $\varepsilon$  can also be thought of as the ratio of the “gain S/N” to the data S/N.

Within the context of our model fitting procedure, the assumed level of gain knowledge can be straightforwardly incorporated using Gaussian priors on the gain parameters. Figure 11 shows the results of fitting to visibility quantities while varying the value of  $\varepsilon$ . We find that noticeable improvements in the posterior constraints start to occur for  $\varepsilon \gtrsim 1$ , and that for  $\varepsilon \gtrsim 10$  the posteriors better approximate the perfect knowledge case (black contours in Figure 11) than they do the no knowledge case (gray contours). This matches our expectation that knowledge of gains begins to inform an overconstrained model as soon as its precision approaches that of the thermal uncertainties. For an underconstrained problem such as imaging using a sparse array, typical regularization imposes much weaker relationships across points in the  $(u, v)$  domain, and partial gain calibration can matter much earlier by providing unique information not sampled by the closure quantities.

While the demonstrations presented here are all done using simulated observations, the recent parameterization of the horizon-scale emission and shadow of the supermassive

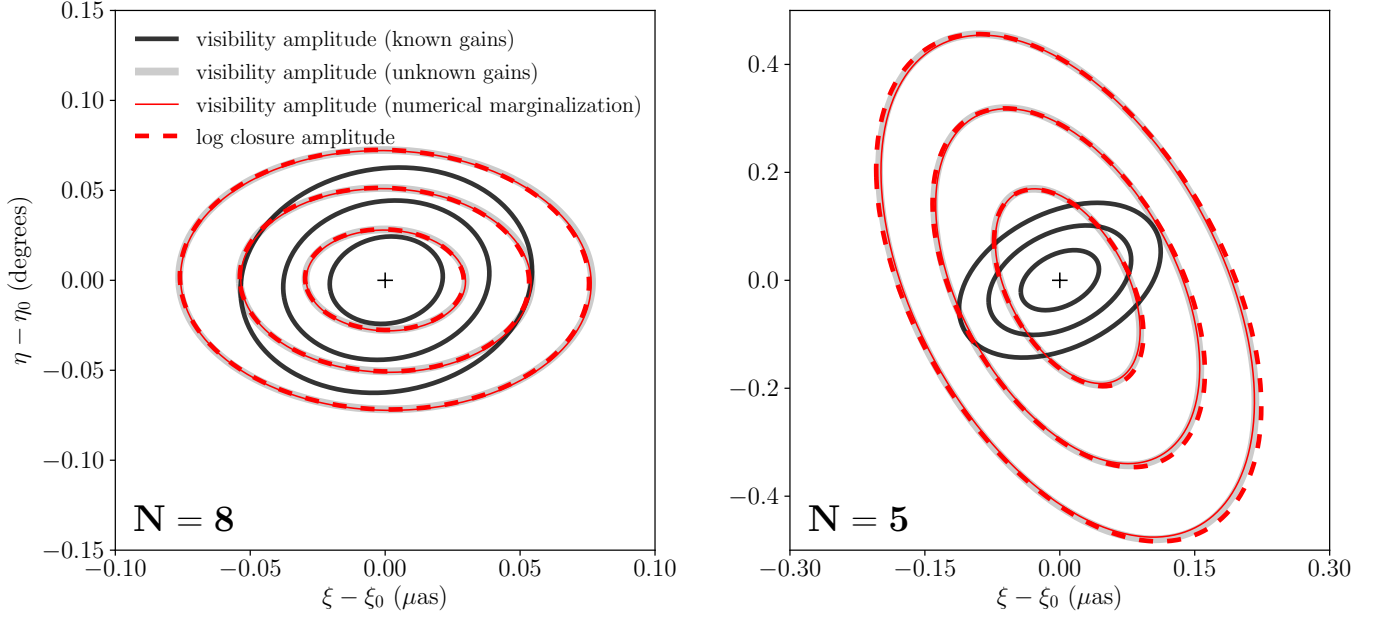


**Figure 10.** Same as Figure 8, but for visibility amplitudes and log closure amplitudes rather than visibility phases and closure phases. Contours enclose 50%, 90%, and 99% of the posterior probability.

black hole in M87 by the [Event Horizon Telescope Collaboration et al. \(2019c\)](#) utilized cross-validation of results across several techniques to handle gain uncertainty. These included explicit semi-analytic marginalization of amplitude gains by Laplace approximation (via THEMIS; [Broderick et al. 2019](#)), minimization of closure phase covariance through selection of a highly sensitive reference antenna (ALMA), and use of diagonalized closure phases and log closure amplitudes by accounting for covariance (via *dynesty*, as described in this work). The multiple approaches resulted in a high degree of consistency as reflected by their posterior parameter distributions. A detailed study of the effects of covariant interferometric errors on imaging and on parameter reconstruction is forthcoming (Pesce et al., *in preparation*).

## 5. SUMMARY

We have explored in detail the statistics of closure phase and closure amplitude for  $S/N \gtrsim 1$ , characteristic of high-frequency radio interferometry where both phase and amplitude calibration have significant uncertainties, and where phase coherence timescales are short relative to the length of a continuous observation. The analysis unifies and clarifies several concepts that have been previously discussed in the literature regarding the independence of closure quantities, the nature and number of statistical degrees of freedom, best practices for constructing and fitting to closure quantities, and the relationship of closure quantities to self calibration and marginalization over unknown gains. Due to the large number of topics covered, we delineate the main statements and findings from this work across three primary topics.

### 1) Formation of closure quantities and non-Gaussian errors:

- Non-Gaussian errors become significant for  $S/N$  below  $\sim 2-5$  for phase, amplitude, and log-amplitude. Reciprocal amplitude is unstable below  $S/N \sim 5$ , which is a motivation to use log-amplitude instead when there is a chance for low- $S/N$  amplitudes to appear in the denominator of an amplitude ratio. ([Appendix A](#))
- The ensemble distribution of measured log-amplitude for known  $S/N$  is fully characterized in terms of moments, from which expected distributions for log closure amplitude can be derived. ([Appendix A](#))
- In practice, a noisy estimate of  $S/N$  prevents a reliable characterization of phase and amplitude errors, particularly for weak signals, and can lead to significant bias from self-selection of data. ([Section 2.4](#))

### 2) The covariance structure for closure quantities – fitting those quantities to a model and characterizing their fundamental degrees of freedom:

- Closure quantities formed from a common set of baseline visibilities are covariant due to shared thermal noise. This must be included for a particular realization to recover both proper  $\chi^2$  statistics and a correct likelihood. ([Section 3.1](#))
- When covariant errors are included, both the  $\chi^2$  and the likelihood (in the Gaussian limit) are independent of the specific minimal set of closure quantities used for the calculation. ([Section 3.1](#))

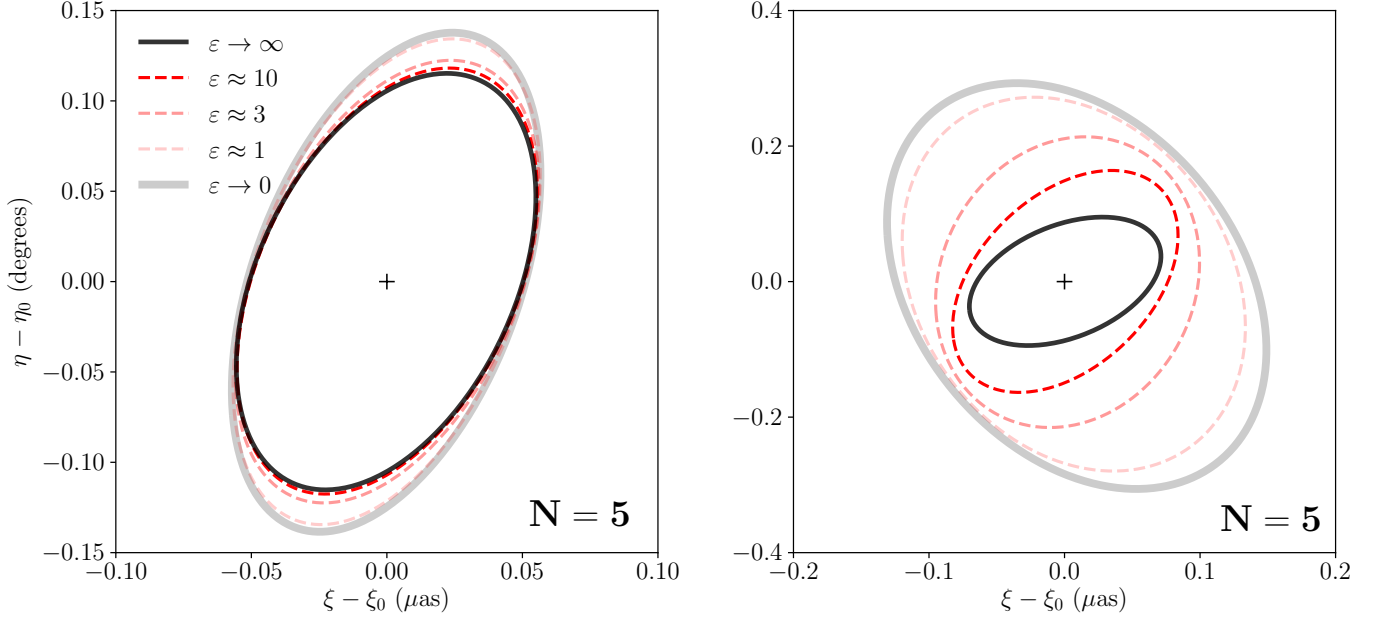


**Figure 11.** *Left:* Posterior contours for fits to visibility phases with varying degrees of prior gain phase knowledge assumed. The gray contour matches the posterior recovered when fitting to closure phases (see Figure 8). *Right:* Same as the left panel, but fitting to visibility amplitudes rather than visibility phases. The contours in both panels enclose 90% of the posterior probability.

Quantity	number	Measured value		Model parameter		Residual		Residual error		
		single	vector	single	vector	single	vector	variance	covariance	design
complex gain	$N$	$\gamma_i$	...	$\hat{\gamma}_i$	...	$\tilde{\gamma}_i$	...	...	...	...
complex visibility	$B$	$V_{ij}$	...	$\hat{V}_{ij}$	...	$\tilde{V}_{ij}$	...	$2\sigma_{V,ij}^2$ (thermal only)	...	...
gain phase	$N$	$\theta_i$	$\boldsymbol{\theta}$	$\hat{\theta}_i$	$\hat{\boldsymbol{\theta}}$	$\tilde{\theta}_i$	$\tilde{\boldsymbol{\theta}}$	$\sigma_{\theta,i}^2$	$\boldsymbol{\Sigma}_{\theta}$	...
visibility phase	$B$	$\phi_{ij}$	$\boldsymbol{\phi}$	$\hat{\phi}_{ij}$	$\hat{\boldsymbol{\phi}}$	$\tilde{\phi}_{ij}$	$\tilde{\boldsymbol{\phi}}$	$\sigma_{ij}^2 + \sigma_{\theta,i}^2 + \sigma_{\theta,j}^2$	$\boldsymbol{\Sigma}_{\phi}$	$\boldsymbol{\Phi}$
closure phase	$T$	$\psi_{ijk}$	$\boldsymbol{\psi}$	$\hat{\psi}_{ijk}$	$\hat{\boldsymbol{\psi}}$	$\tilde{\psi}_{ijk}$	$\tilde{\boldsymbol{\psi}}$	$\sigma_{ijk}^2$	$\boldsymbol{\Sigma}_{\psi}$	$\boldsymbol{\Psi}$
gain amplitude	$N$	$G_i$	...	$\hat{G}_i$	...	$\tilde{G}_i$	...	...	...	...
visibility amplitude	$B$	$A_{ij}$	...	$\hat{A}_{ij}$	...	$\tilde{A}_{ij}$	...	...	...	...
closure amplitude	$Q$	$C_{ijkl}$	...	$\hat{C}_{ijkl}$	...	$\tilde{C}_{ijkl}$	...	...	...	...
log gain amplitude	$N$	$g_i$	$\mathbf{g}$	$\hat{g}_i$	$\hat{\mathbf{g}}$	$\tilde{g}_i$	$\tilde{\mathbf{g}}$	$\sigma_{g,i}^2$	$\boldsymbol{\Sigma}_g$	...
log visibility amplitude	$B$	$a_{ij}$	$\mathbf{a}$	$\hat{a}_{ij}$	$\hat{\mathbf{a}}$	$\tilde{a}_{ij}$	$\tilde{\mathbf{a}}$	$\sigma_{ij}^2 + \sigma_{g,i}^2 + \sigma_{g,j}^2$	$\boldsymbol{\Sigma}_a$	$\mathbf{A}$
log closure amplitude	$Q$	$c_{ijkl}$	$\mathbf{c}$	$\hat{c}_{ijkl}$	$\hat{\mathbf{c}}$	$\tilde{c}_{ijkl}$	$\tilde{\mathbf{c}}$	$\sigma_{ijkl}^2$	$\boldsymbol{\Sigma}_c$	$\mathbf{C}$

**Table 2.** Notation used in this paper. Measured values reflect contributions from thermal noise and systematic errors. The residual error represents the expected covariance across a set of simultaneously observed residual quantities (measured minus model values). For visibilities, the residual covariance includes contributions from both thermal (statistical) and gain (systematic) errors in the general case. At high S/N, the variance for phase and log-amplitude are equal, thus we use the same symbol  $\sigma_{ij}^2 \approx \sigma_{V,ij}^2/A_{ij}$  for notational simplicity.  $\sigma_{V,ij}^2$  reflects the thermal noise in one component of the complex visibility, and it is known a priori to high precision.

- In the limit of equal S/N on all baselines, the  $\chi^2$  for a specific minimal set reduces to an evaluation over all closure quantities weighted equally, scaled to the appropriate degrees of freedom. (Appendix C)
- If closure quantities are assumed to be independent and the covariance structure is ignored, results do depend on the specific choice of minimal set. Certain selections can be chosen to minimize off-diagonal terms

in the covariance matrix, but this choice depends on the specific arrangement of baseline S/N. (Section 3.2, Figure 9 of Section 4)

- Two different direct constructions for selecting non-redundant sets of closure amplitudes are given. They verify explicitly the expected  $N(N-3)/2$  independent degrees of freedom contained in the closure amplitudes. (Section 3.2 and Appendix B.3)

- A unified matrix construction for creating visibilities and closure quantities is given, which systematically builds up design matrices for increasing station number. These are used to derive the covariance and other relationships across different quantities. ([Appendix B](#))

3) Relationship of closure information to station gain information, and behavior in the limit of completely known gains, partially known gains, and completely unknown gains:

- Under a model for systematic station-based gain error, residual visibility phase and log amplitude also assume a covariance structure with non-zero diagonal elements due to gain model error. ([Section 4.1](#))
- Using this covariance structure for visibilities is equivalent to explicitly marginalizing over additional free gain parameters under a Gaussian prior. Such analytic marginalization may not be possible for more complicated prior distributions. ([Appendix C.5](#))
- In the limit of small thermal error compared to gain error, the  $\chi^2$  derived from visibility measurements reduces to the  $\chi^2$  derived from only closure quantities, after accounting for covariance. Thus, the closure quantities contain all non-station based information. ([Appendix C.4](#))
- We apply the likelihood constructions introduced in this paper toward direct sampling of the posterior dis-

tribution of a simple source model and simulated observation. We confirm that the inferred parameter posterior derived using closure quantities matches that derived using baseline visibilities in the limit of unknown gains, and that the uncertainties are larger than those derived under known gain calibration, reflecting the relative loss of information. ([Section 4](#))

- Under modeling of partially known gains, with systematic station gain uncertainty comparable to that from baseline thermal noise, we see that the model posterior distribution transitions smoothly between the case of perfectly calibrated corresponding to zero gain error, and completely unknown calibration using only closure quantities. ([Section 4.5](#))

#### ACKNOWLEDGMENTS

The authors would like to thank Jim Moran, Geoff Bower, Ramesh Narayan, Kazunori Akiyama, Katie Bouman, Christian Brinkerink, Avery Broderick, and Josh Speagle for helpful discussions, comments, and ideas. We thank the National Science Foundation (AST-1440254, AST-1614868) and the Gordon and Betty Moore Foundation (GBMF-5278) for financial support of this work. This work was supported in part by the Black Hole Initiative at Harvard University, which is supported by a grant from the John Templeton Foundation and the Gordon and Betty Moore Foundation.

#### REFERENCES

- Blackburn, L., Chan, C.-k., Crew, G. B., et al. 2019, [ApJ](#), **882**, 23
- Broderick, A., et al. 2019, *in preparation*
- Chael, A. A., Johnson, M. D., Bouman, K. L., et al. 2018, [ApJ](#), **857**, 23
- Christian, P., & Psaltis, D. 2019, arXiv e-prints, [arXiv:1909.04681](#)
- Event Horizon Telescope Collaboration, et al. 2019a, [ApJ](#), **875**, L2
- . 2019b, [ApJ](#), **875**, L3
- . 2019c, [ApJ](#), **875**, L6
- Ireland, M. J. 2013, [MNRAS](#), **433**, 1718
- Jennison, R. C. 1958, [MNRAS](#), **118**, 276
- Kulkarni, S. R. 1989, [AJ](#), **98**, 1112
- Kulkarni, S. R., Prasad, S., & Nakajima, T. 1991, [J. Opt. Soc. Am. A](#), **8**, 499
- Lannes, A. 1990a, in *Proc. SPIE*, Vol. 1351, *Digital Image Synthesis and Inverse Optics*, ed. A. F. Gmitro, P. S. Idell, & I. J. Lahaie, 38
- Lannes, A. 1990b, [J. Opt. Soc. Am. A](#), **7**, 500
- Lannes, A. 1991, *Inverse Problems*, **7**, 261
- Lapidoth, A., & Moser, S. M. 2003, [IEEE Trans. Inf. Theory](#), **49**, 2426
- Martinache, F. 2010, [ApJ](#), **724**, 464
- Massi, M., Tofani, G., & Comoretto, G. 1991, [A&A](#), **251**, 732
- Pav, S. E. 2015, arXiv e-prints, [arXiv:1503.06266](#)
- Pearson, T. J., & Readhead, A. C. S. 1984, [ARA&A](#), **22**, 97
- Readhead, A. C. S., Walker, R. C., Pearson, T. J., & Cohen, M. H. 1980, [Nature](#), **285**, 137
- Readhead, A. C. S., & Wilkinson, P. N. 1978, [ApJ](#), **223**, 25
- Rogers, A. E. E., Doeleman, S. S., & Moran, J. M. 1995, [AJ](#), **109**, 1391
- Rogers, A. E. E., Hinteregger, H. F., Whitney, A. R., et al. 1974, [ApJ](#), **193**, 293
- Speagle, J. S. 2019, arXiv e-prints, [arXiv:1904.02180](#)
- Thompson, A. R., Moran, J. M., & Swenson, George W., J. 2017, *Interferometry and Synthesis in Radio Astronomy*, 3rd Edition (Springer)
- Twiss, R. Q., Carter, A. W. L., & Little, A. G. 1960, *The Observatory*, **80**, 153
- van Cittert, P. H. 1934, [Physica](#), **1**, 201
- Zernike, F. 1938, [Physica](#), **5**, 785

## APPENDIX

## A. DISTRIBUTIONS DUE TO THERMAL NOISE

Here we discuss the statistical distributions of measured amplitude and phase quantities used for model fitting, quality of the normal distribution approximations, and influence of the estimation of an intrinsic signal-to-noise parameter  $\check{\rho}$ . In the thermal noise dominated regime the fundamental measured quantity, complex correlation coefficient  $r$ , follows circularly-symmetric complex normal distribution with mean  $\check{\rho}\sigma_r$ . Without loss of generality we choose our coordinates such that the mean of the complex correlation distribution is real. An associated standard deviation of both real and imaginary components  $\sigma_r$  can be computed from first principles (Thompson et al. 2017). Hence, it is useful to work with the normalized complex random variable  $r/\sigma_r$ , with unit standard deviation (Figure 12). Probability densities for closure quantities, as shown in Figure 1 and Figure 2, can then be derived from the ones presented here with elementary operations such as convolution.

## A.1. Phase and amplitude distributions

The correlation coefficient phase  $\phi$  is the argument of a circular complex normal variable and as such obeys the following circular distribution (Thompson et al. 2017)

$$p(\phi|\check{\rho}) = \frac{1}{2\pi} \exp\left(-\frac{\check{\rho}^2}{2}\right) \left\{ 1 + \sqrt{\frac{\pi}{2}} \check{\rho} \cos \phi \exp\left(\frac{\check{\rho}^2 \cos^2 \phi}{2}\right) \times \left[ 1 + \text{Erf}\left(\frac{\check{\rho} \cos \phi}{\sqrt{2}}\right) \right] \right\}. \quad (\text{A1})$$

We choose the coordinates in such a way that the true visibility phase is zero and denote the error function with Erf. Examples showing the probability density  $p(\phi|\check{\rho})$  for different values of  $\check{\rho}$  are shown in the top left panel of Figure 13. This somewhat complicated distribution can be approximated either by a normal distribution (dashed lines in Figure 13),

$$p_N(\phi|\check{\rho}) = \frac{\check{\rho}}{\sqrt{2\pi}} \exp\left(-\frac{\phi^2 \check{\rho}^2}{2}\right), \quad \sigma_N^2 = \frac{1}{\check{\rho}^2}, \quad (\text{A2})$$

or by the von Mises distribution (dotted lines in Figure 13) (Christian & Psaltis 2019),

$$p_M(\phi|\check{\rho}) = \frac{\check{\rho} \exp(\check{\rho}^2 \cos \phi)}{2\pi I_0(\check{\rho}^2/2)}, \quad \sigma_M^2 = 1 - \frac{I_1(\check{\rho}^2/2)}{I_0(\check{\rho}^2/2)}. \quad (\text{A3})$$

which outperforms the normal distribution for low S/N.

For a given model  $\check{\rho}$ , the measured normalized correlation coefficient amplitude  $\rho = |r/\sigma_r| \geq 0$  follows a Rice distribution,

$$p(\rho|\check{\rho}) = \rho \exp\left(-\frac{\rho^2 + \check{\rho}^2}{2}\right) I_0(\rho\check{\rho}), \quad (\text{A4})$$

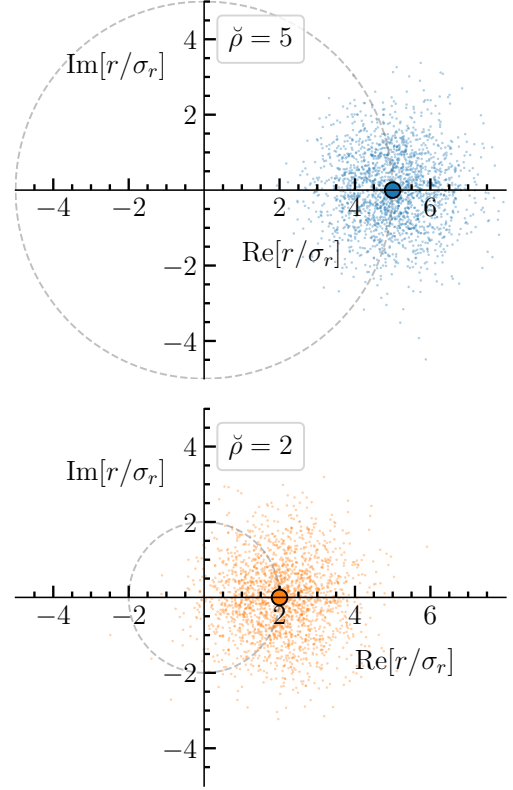


**Figure 12.** Two thousand random realizations of the measured complex correlation coefficient  $r/\sigma_r$  given intrinsic signal-to-noise  $\check{\rho} = 2$  and 5.

where  $I_0$  is a modified Bessel function of the first kind with order zero. Distributions of visibility amplitude are shown in Figure 13 (top right panel). Dashed lines represent a normal distribution approximation with mean  $m^2 = (\check{\rho}^2 + 1)$  and unit standard deviation, which is accurate in the limit  $\check{\rho} \rightarrow \infty$ . The normal approximation can not properly handle strictly non-negative random variables, which becomes a problem at low S/N. The mean of the correlation amplitude is also positively biased with respect to  $\check{\rho}$  due to its noise contribution, and we find  $E[\rho] = 2.272$  for  $\check{\rho} = 2$  and  $E[\rho] = 5.101$  for  $\check{\rho} = 5$ , which illustrates why debiasing is important for incoherent averaging over many realizations, and for estimating  $\check{\rho}$  from low S/N data.

When working with closure amplitudes, we need to utilize the reciprocal amplitudes  $y = 1/\rho$ , distributed according to

$$p(y|\check{\rho}) = \frac{1}{y^3} \exp\left(-\frac{1/y^2 + \check{\rho}^2}{2}\right) I_0\left(\frac{\check{\rho}}{y}\right). \quad (\text{A5})$$

Although this distribution can be approximated at high-S/N as a normal distribution with mean  $m^2 = (\check{\rho}^2 + 1)^{-1}$  and stan-



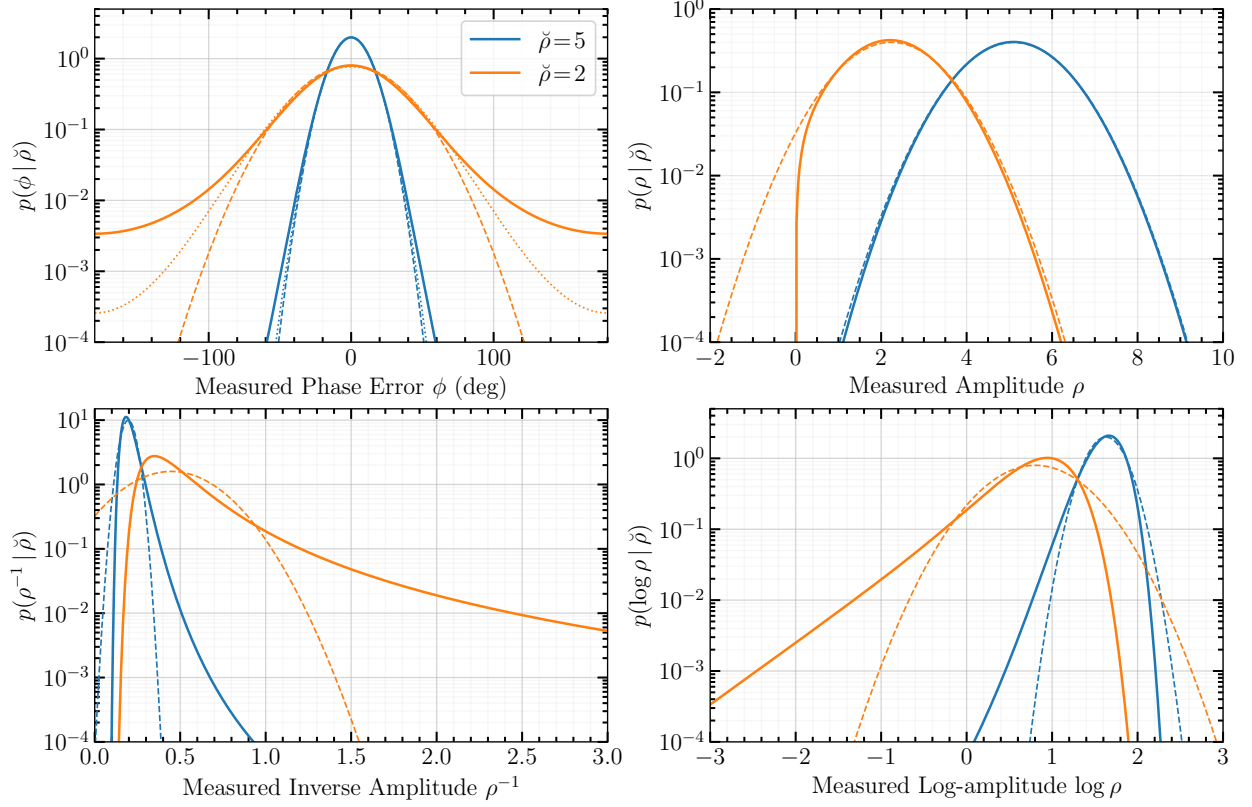


**Figure 13.** Analytic distributions of phase and amplitude quantities (continuous lines). Normal distribution approximations, exact in the  $\check{\rho} \rightarrow \infty$  limit, are shown with dashed lines. For the visibility phase (top left panel), the von Mises distribution approximation is shown with a dotted line. All presented approximations assume knowledge of a hidden parameter  $\check{\rho}$ , which in general must be estimated from noisy measurements.

dard deviation  $\check{\rho}^{-2}$  (Figure 13 bottom left), the probability distribution exhibits heavy tails at the low S/N, related to inversion of potentially arbitrarily small amplitude. The fact that amplitude is always positive is one indication that log amplitude might be a more natural space in which to characterize the distribution. Another benefit of using log amplitude is that amplitude and squared-amplitude (a more natural quantity for incoherent sums of Gaussian components) are simply related. Logarithms of the correlation amplitude  $z = \log \rho$  (log denotes a natural logarithm) obey a following log-Rice distribution

$$p(z|\check{\rho}) = \exp\left(2z - \frac{\check{\rho}^2}{2} - \frac{\exp 2z}{2}\right) I_0(\check{\rho} \exp z). \quad (\text{A6})$$

The distributions of the logarithm of amplitude for different  $\check{\rho}$  are shown in Figure 13, bottom right. Moments of the log-Rice distribution are treatable analytically, and the distribution can be approximated with a normal distribution of mean  $m = 0.5 \log(\check{\rho}^2 + 1)$  and standard deviation  $1/\check{\rho}$ . A more general exact treatment of incoherent averages of  $M$  amplitude measurements follows.

#### A.2. Log amplitude ensemble distribution

Consider a set of  $M$  independent complex visibility measurements  $v_i$  where each complex component has thermal noise of 1. Thus  $v_i = \check{\rho}_i + n_i$  where  $\check{\rho}_i$  is some expected signal-to-noise ratio for each measurement and  $n_i$  is a Gaussian complex random variable with  $\sigma = 1$  for each component. The sum-squared amplitudes follow a  $\chi^2$  distribution with  $2M$  degrees of freedom. This will be a noncentral  $\chi^2$  distribution if it includes a nonzero expected source contribution.

$$x = \sum_i |v_i|^2 \quad f(x) = \chi_{2M, \lambda}^2 \quad (\text{A7})$$

where  $\lambda$  is the noncentrality parameter,

$$\lambda = \sum_i |\check{\rho}_i|^2 \quad (\text{A8})$$

The expectation value of  $\log x$  is,

$$\mathbb{E}[\log x] = g_M(\lambda) \quad (\text{A9})$$

and  $g(\cdot)$  is the function (Lapidoth & Moser 2003),

$$g(\lambda) = \begin{cases} \log \lambda - \text{Ei} \left[ -\frac{\lambda}{2\sigma^2} \right] & (\text{if } \lambda > 0) \\ + \sum_{j=1}^{M-1} (-1)^j \left[ e^{-\lambda} (j-1)! - \frac{(M-1)!}{j(M-1-j)!} \right] \left( \frac{1}{\lambda} \right)^j & \\ \log 2\sigma^2 - \gamma + \sum_{j=1}^{M-1} \frac{1}{j} & (\text{if } \lambda = 0) \end{cases} \quad (\text{A10})$$

where  $\gamma \approx 0.577$  is the Euler-Mascheroni constant and Ei is the exponential integral. We have introduced  $\sigma$  for the case where amplitudes are uniformly scaled away from  $\sigma = 1$ . From this the expectation value  $\text{E}[\log \sqrt{x}] = \text{E}[\log x]/2$  is easy to calculate, for example in the case of a single Rice-distributed complex visibility (where “measured”  $\rho = |v|$ )

$$\text{E}[\log \rho] = \log \check{\rho} - \text{Ei} \left[ -\frac{\check{\rho}^2}{2} \right]. \quad (\text{A11})$$

The log closure amplitude  $c$  is formed from linear combination of four log amplitudes  $A, B, C, D$ ,

$$c = A + B - C - D \quad (\text{A12})$$

so that the expectation value (from which a bias is derived) is trivial,

$$\text{E}[c] = \text{E}[A] + \text{E}[B] - \text{E}[C] - \text{E}[D] \quad (\text{A13})$$

To characterize the distribution of measured closure amplitudes, we require additional moments beyond the first moment (bias). For a multivariate Gaussian approximation suitable for least squares fitting of log closure quantities with known covariance, we need to estimate the second moment of each log amplitude. High order moments of the log non-central  $\chi^2$  distribution can be derived as Poisson-weighted infinite series of polygamma functions  $\psi^{(m)}(z)$  (Pav 2015),

$$\text{E}[x^k] = \sum_{j=0}^{\infty} \frac{e^{-\lambda/2} (\lambda/2)^j}{j!} \mu'_{k_2 M + 2j} \quad (\text{A14})$$

where  $\mu'_{k_2 M + 2j}$  is the  $k^{\text{th}}$  moment (not central moment) of a log chi-square ( $\lambda = 0$ ) distribution with  $2M + 2j$  degrees of freedom,

$$\mu'_n = \kappa_n + \sum_{m=1}^{n-1} \binom{n-1}{m-1} \kappa_m \mu'_{n-m} \quad (\text{A15})$$

$$\kappa_n = \begin{cases} \log 2 + \psi(M+j) & n = 1 \\ \psi^{(n-1)}(M+j) & n > 1 \end{cases} \quad (\text{A16})$$

in terms of cumulants  $\kappa_n$ . Note that the second and third cumulants are equal to the corresponding central moments. The cumulants in terms of noncentral moments are,

$$\kappa_n = \mu'_n - \sum_{m=1}^{n-1} \binom{n-1}{m-1} \kappa_m \mu'_{n-m} \quad (\text{A17})$$

For a single log-central  $\chi^2$  distribution of 2 degrees of freedom (i.e. an exponential distribution with mean value 2), the first and second cumulants are particularly simple,

$$\text{E}[\log \chi_2^2] = \log 2 + \psi(1) = \log 2 - \gamma \quad (\text{A18})$$

$$\text{var}(\log \chi_2^2) = \psi^1(1) = \frac{\pi^2}{6} \quad (\text{A19})$$

which are the same as the cumulants for a log-Rayleigh distribution scaled appropriately by a factor of two.

Recurrence relationships for polygamma can be used to quickly derive cumulants, including higher order cumulants, of the log-central  $\chi^2$  distribution of  $2M$  degrees of freedom. Aside from  $\kappa_1$ , the higher order cumulants approach zero as  $M \rightarrow \infty$ . We see that calculating cumulants at increasing number of degrees of freedom is simply adding one more term to the series.

$$\kappa_1 = \log 2 - \gamma + \sum_{k=1}^{M-1} \frac{1}{k} \quad (\text{A20})$$

$$\kappa_2 = \frac{\pi^2}{6} - \sum_{k=1}^{M-1} \frac{1}{k^2} \quad (\text{A21})$$

$$\kappa_3 = -2\zeta(3) + \sum_{k=1}^{M-1} \frac{2}{k^3} \quad (\text{A22})$$

$$\kappa_4 = \frac{\pi^4}{15} - \sum_{k=1}^{M-1} \frac{6}{k^4} \quad (\text{A23})$$

or, more generally,

$$\frac{\psi^{(n-1)}(M)}{(-1)^n (n-1)!} = \zeta(n) - \sum_{k=1}^{M-1} \frac{1}{k^n} = \sum_{k=M}^{\infty} \frac{1}{k^n} \quad (\text{A24})$$

These relatively simple expressions are for the cumulants of a log central  $\chi^2$  distribution. They must be converted into moments of a *noncentral* distribution by summing over the appropriate Poisson mixture (Equation A14), which depends on the noncentrality parameter. The noncentral moments can then be converted back into cumulants of the noncentral distribution to build cumulants of the log closure amplitude distribution. For a log closure amplitude  $c = A + B - C - D$ , the cumulants of  $c$  are formed as,

$$\kappa_{c,1} = \kappa_{A,1} + \kappa_{B,1} - \kappa_{C,1} - \kappa_{D,1} \quad (\text{mean}) \quad (\text{A25})$$

$$\kappa_{c,2} = \kappa_{A,2} + \kappa_{B,2} + \kappa_{C,2} + \kappa_{D,2} \quad (\text{variance}) \quad (\text{A26})$$

$$\kappa_{c,3} = \kappa_{A,3} + \kappa_{B,3} - \kappa_{C,3} - \kappa_{D,3} \quad (\text{skew} \times \kappa_2^{3/2}) \quad (\text{A27})$$

$$\kappa_{c,4} = \kappa_{A,4} + \kappa_{B,4} + \kappa_{C,4} + \kappa_{D,4} \quad (\text{ex. kurtosis} \times \kappa_2^2) \quad (\text{A28})$$

and so on. Figure 14 shows the first four moments calculated this way using a finite number of nonzero terms from the Poisson mixture, and compared to a Monte Carlo estimation.

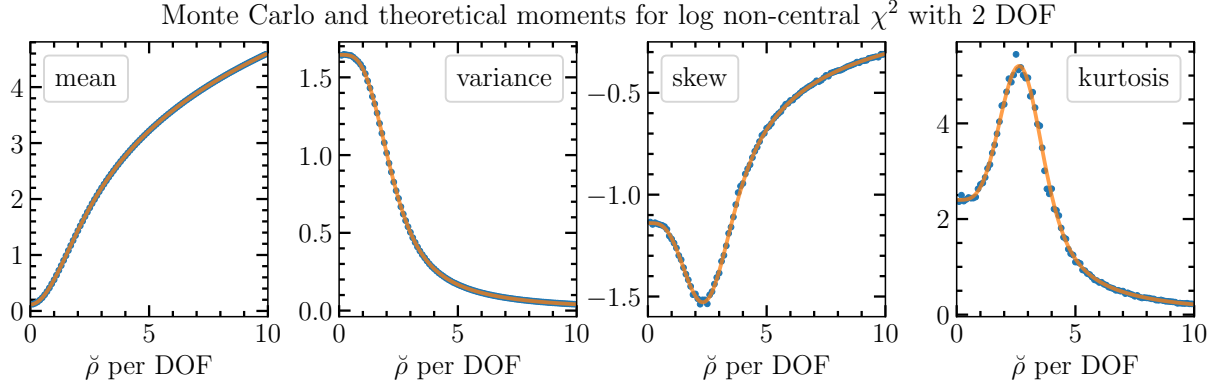


**Figure 14.** Moments of the log-noncentral  $\chi^2$  distribution (2 degrees of freedom) as a function of signal-to-noise. Blue dots correspond to a Monte Carlo estimation, while orange lines correspond to the moment expansion (Equation A14) over a finite number of Poisson terms. The noncentral  $\chi^2$  distribution itself is not well captured by a small number of moments (due to the tail), but for log closure amplitude, the propagated moments (A26–A28) can be used to fit to good approximations such as an exponentially modified Gaussian distribution.

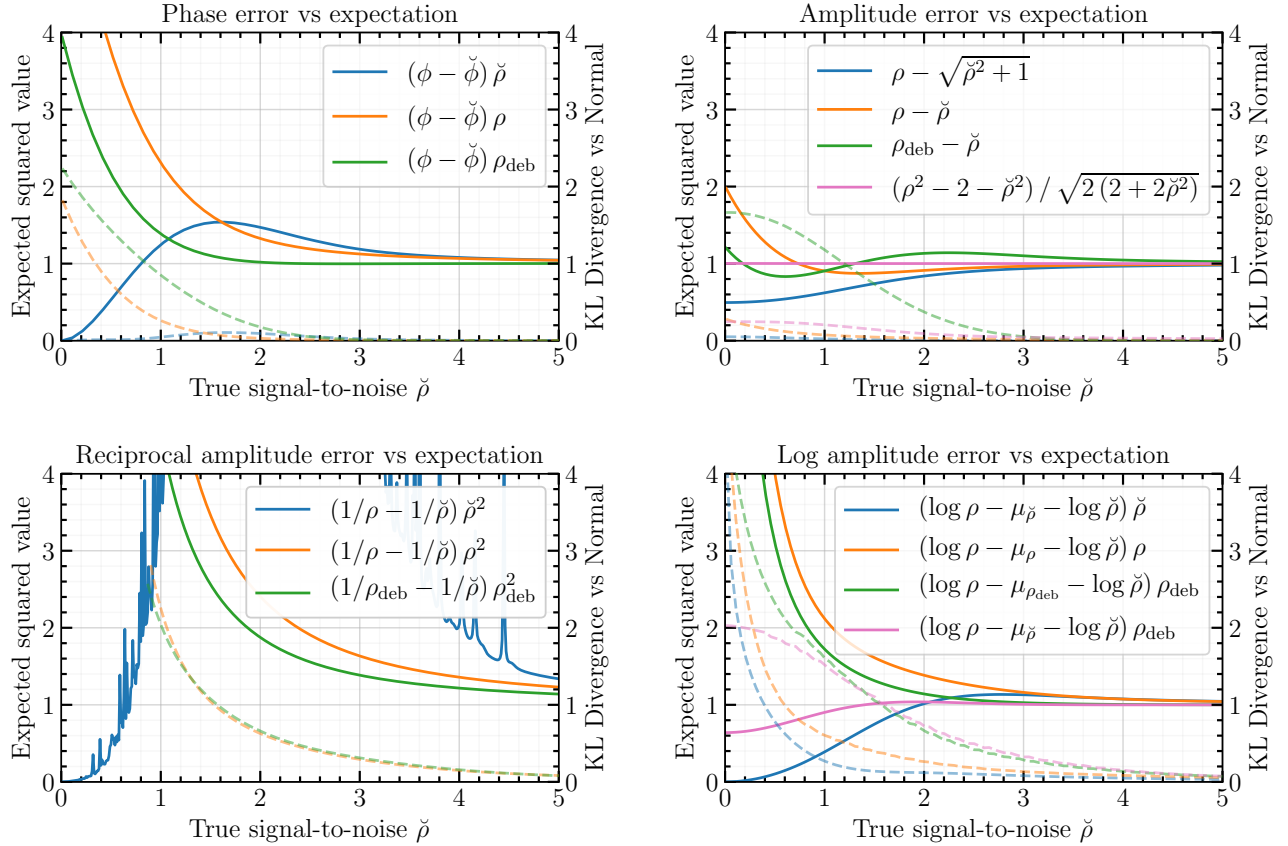


**Figure 15.** The four panels show the quality of the Normal approximation for different phase and amplitude distributions as a function of model S/N. Solid lines show the expected squared value of the normalized residual quantity (expected reduced  $\chi^2$ ) from the legend, while dashed lines show the relative entropy (Kullback-Leibler divergence) between the true distribution of each quantity and a standard Normal distribution. For example the values at  $\tilde{\rho} = 2$  reflect an ensemble of complex visibilities with intrinsic  $\tilde{\rho} = 2$  and measured  $\rho = |r/\sigma_r|$  for each random realization (see Figure 12). The orange line in the top left figure thus corresponds to an expected squared deviation in measured phase  $\phi = \text{Arg}[\rho]$  away from the truth value  $\check{\phi}$ , where the deviation is normalized by an empirical error estimate  $\sigma_\phi = 1/\rho$ . Other curves show different error estimates based on the model  $\tilde{\rho}$  (which is typically not known in a real observation), or a noise-debiased estimate  $\rho_{\text{deb}} = \sqrt{\rho^2 - 1}$ . For log amplitude,  $\mu$  corresponds to the small expected bias from Equation A11.

### A.3. Quality of distribution approximations

The true underlying value of  $\check{\rho}$  remains generally unknown and our ability to estimate  $\check{\rho}$  will influence the quality of our derived distribution for the measured value, in addition to possible mismatch due to any approximations used. In Figure 15 we evaluate the influence of both these effects using a  $\chi^2$  test and also by calculating the Kullback-Leibler divergence between the ground truth and a normal distribution characterized by the two approximated moments.

Given knowledge of true  $\check{\rho}$ , it is possible in principle to achieve perfect statistics due to full knowledge of the distribution, rather than the high S/N approximations used in the figure. However this does not extend to the empirical (realistic) estimators. Furthermore, we see that the estimator with  $\chi_r^2$  closest to 1 is not always the one with the best Gaussianity according to the KL divergence. Lastly, although reciprocal amplitude is very difficult to characterize due to values near zero – motivating the use of log amplitude, visibility amplitude itself is comparatively well behaved and easy to approximate, even to low S/N.

## B. DESIGN AND COVARIANCE MATRIX CONSTRUCTION

### B.1. Baseline phase and amplitude matrices

A pair of complex visibilities may share a station, so station-based gain effects result in covariances between visibility measurements. The covariance between two visibility phase measurements  $\phi_{ij}$  and  $\phi_{k\ell}$  can be expressed as

$$\begin{aligned} \text{Cov}(\phi_{ij}, \phi_{k\ell}) = & \sigma_{ij}^2 (\delta_{ik}\delta_{j\ell} - \delta_{i\ell}\delta_{jk}) \\ & + \sigma_{\theta,i}^2 (\delta_{ik} - \delta_{i\ell}) - \sigma_{\theta,j}^2 (\delta_{jk} - \delta_{j\ell}), \end{aligned} \quad (\text{B29})$$

where  $\sigma_{ij}^2$  is the thermal variance of the visibility phase measurement  $\phi_{ij}$ ,  $\sigma_{\theta,i}^2$  is the gain phase variance for station  $i$ , and  $\delta_{ij}$  is the Kronecker delta. A similar expression holds for the covariance between two log visibility amplitude measurements  $a_{ij}$  and  $a_{k\ell}$ ,

$$\begin{aligned} \text{Cov}(a_{ij}, a_{k\ell}) = & \sigma_{ij}^2 (\delta_{ik}\delta_{j\ell} + \delta_{i\ell}\delta_{jk}) \\ & + \sigma_{g,i}^2 (\delta_{ik} + \delta_{i\ell}) + \sigma_{g,j}^2 (\delta_{jk} + \delta_{j\ell}), \end{aligned} \quad (\text{B30})$$

where  $\sigma_{ij}^2$  is the thermal variance of the log visibility amplitude measurement  $a_{ij}$  and  $\sigma_{g,i}^2$  is the log gain amplitude variance for station  $i$ .

We can see from Equation B29 and Equation B30 that the visibility measurement covariances separate into baseline-based and station-based terms. We can thus write the visibility phase covariance matrix  $\Sigma_\phi$  as

$$\Sigma_\phi = \Phi \Sigma_\theta \Phi^\top + \mathbf{S}_\phi. \quad (\text{B31})$$

The  $\Sigma_\theta$  and  $\mathbf{S}_\phi$  matrices are  $N \times N$  and  $B \times B$  diagonal matrices constructed from the individual station gain phase variances and visibility phase variances, respectively. The visibility phase “design matrix”  $\Phi$  is rectangular in general, with  $B$  rows and  $N$  columns, and provides a mapping from the station-based representation to the baseline-based representation. Each row of  $\Phi$  contains only two nonzero entries, the first being a 1 and the second being a  $-1$ . There are  $B$  different ways of writing a length- $N$  row in this fashion, and these constitute the  $B$  rows of the matrix. The ordering of these rows depends on the chosen baseline ordering scheme. In this section we assume a “second station first” baseline ordering scheme, which increments the visibility phases via a nested loop method. The “inner loop” iterates through the second station in increasing order and the “outer loop” iterates through the first station in increasing order. An example such ordering would be  $(\phi_{12}, \phi_{13}, \phi_{14}, \dots, \phi_{1N}, \phi_{23}, \phi_{24}, \dots, \phi_{2N}, \phi_{34}, \dots, \phi_{N-1,N})$ , where the indices here correspond to the two stations forming each baseline.

For a general  $N$ -station array with  $N > 2$ , we present the following recursive relationship for the visibility phase design matrix:

$$\Phi_N = \begin{pmatrix} \mathbf{1} & -\mathbf{I}_{N-1} \\ \mathbf{0} & \Phi_{N-1} \end{pmatrix}, \quad (\text{B32})$$

where  $\mathbf{1}$  is a  $(N-1) \times 1$  vector containing only 1’s,  $\mathbf{0}$  is a  $\binom{N-1}{2} \times 1$  vector containing only 0’s,  $\mathbf{I}_{N-1}$  is the identity matrix of rank  $N-1$ , and  $\Phi_{N-1}$  is the visibility phase design matrix for an array with  $N-1$  stations. The rank of  $\Phi_N$  is equal to  $N-1$ . Table 3 lists examples of  $\Phi$  and the corresponding  $\Sigma_\phi$  matrices.

The log visibility amplitude design matrix  $\mathbf{A}$  shares the same structure as the visibility phase design matrix, with the only difference being that the negative elements of  $\Phi$  become positive for  $\mathbf{A}$ . As a result, for  $N > 2$  the rank of  $\mathbf{A}_N$  for the log visibility amplitudes is equal to  $N$ . Table 4 lists examples of log visibility amplitude design and covariance matrices.

### B.2. Closure phase matrices

It is possible for two closure triangles to have a baseline in common, so in general two closure phase measurements may be covariant. The covariance between two closure phase measurements  $\psi_{ijk}$  and  $\psi_{lmn}$  can be expressed as

$$\begin{aligned} \text{Cov}(\psi_{ijk}, \psi_{lmn}) = & \sigma_{ij}^2 (\delta_{il}\delta_{jm} + \delta_{im}\delta_{jn} + \delta_{in}\delta_{jl}) \\ & - \sigma_{ij}^2 (\delta_{i\ell}\delta_{jn} + \delta_{im}\delta_{j\ell} + \delta_{in}\delta_{jm}) \\ & + \sigma_{jk}^2 (\delta_{jl}\delta_{km} + \delta_{jm}\delta_{kn} + \delta_{jn}\delta_{k\ell}) \\ & - \sigma_{jk}^2 (\delta_{j\ell}\delta_{kn} + \delta_{jm}\delta_{k\ell} + \delta_{jn}\delta_{km}) \\ & + \sigma_{ik}^2 (\delta_{i\ell}\delta_{kn} + \delta_{im}\delta_{k\ell} + \delta_{in}\delta_{km}) \\ & - \sigma_{ik}^2 (\delta_{i\ell}\delta_{km} + \delta_{im}\delta_{kn} + \delta_{in}\delta_{k\ell}). \end{aligned} \quad (\text{B33})$$

Matrix	Shape	Number of stations ( $N$ )	
		$N = 2$	$N = 3$
$\Sigma_\theta$	$N \times N$	$\begin{pmatrix} \sigma_{\theta,1}^2 & 0 \\ 0 & \sigma_{\theta,2}^2 \end{pmatrix}$	$\begin{pmatrix} \sigma_{\theta,1}^2 & 0 & 0 \\ 0 & \sigma_{\theta,2}^2 & 0 \\ 0 & 0 & \sigma_{\theta,3}^2 \end{pmatrix}$
$\mathbf{S}_\phi$	$B \times B$	$\begin{pmatrix} \sigma_{12}^2 \end{pmatrix}$	$\begin{pmatrix} \sigma_{12}^2 & 0 & 0 \\ 0 & \sigma_{13}^2 & 0 \\ 0 & 0 & \sigma_{23}^2 \end{pmatrix}$
$\Phi$	$B \times N$	$\begin{pmatrix} 1 & -1 \end{pmatrix}$	$\begin{pmatrix} 1 & -1 & 0 \\ 1 & 0 & -1 \\ 0 & 1 & -1 \end{pmatrix}$
$\Sigma_\phi$	$B \times B$	$\begin{pmatrix} \sigma_{12}^2 + \sigma_{\theta,1}^2 + \sigma_{\theta,2}^2 \end{pmatrix}$	$\begin{pmatrix} \sigma_{12}^2 + \sigma_{\theta,1}^2 + \sigma_{\theta,2}^2 & \sigma_{\theta,1}^2 & -\sigma_{\theta,2}^2 \\ \sigma_{\theta,1}^2 & \sigma_{13}^2 + \sigma_{\theta,1}^2 + \sigma_{\theta,3}^2 & \sigma_{\theta,3}^2 \\ -\sigma_{\theta,2}^2 & \sigma_{\theta,3}^2 & \sigma_{23}^2 + \sigma_{\theta,2}^2 + \sigma_{\theta,3}^2 \end{pmatrix}$

**Table 3.** Visibility phase design and covariance matrices for 2- and 3-element arrays, along with matrices relevant for their construction. Here,  $B = \binom{N}{2}$  is the number of baselines.

Matrix	Shape	Number of stations ( $N$ )	
		$N = 2$	$N = 3$
$\Sigma_g$	$N \times N$	$\begin{pmatrix} \sigma_{g,1}^2 & 0 \\ 0 & \sigma_{g,2}^2 \end{pmatrix}$	$\begin{pmatrix} \sigma_{g,1}^2 & 0 & 0 \\ 0 & \sigma_{g,2}^2 & 0 \\ 0 & 0 & \sigma_{g,3}^2 \end{pmatrix}$
$\mathbf{S}_a$	$B \times B$	$\begin{pmatrix} \sigma_{12}^2 \end{pmatrix}$	$\begin{pmatrix} \sigma_{12}^2 & 0 & 0 \\ 0 & \sigma_{13}^2 & 0 \\ 0 & 0 & \sigma_{23}^2 \end{pmatrix}$
$\mathbf{A}$	$B \times N$	$\begin{pmatrix} 1 & 1 \end{pmatrix}$	$\begin{pmatrix} 1 & 1 & 0 \\ 1 & 0 & 1 \\ 0 & 1 & 1 \end{pmatrix}$
$\Sigma_a$	$B \times B$	$\begin{pmatrix} \sigma_{12}^2 + \sigma_{g,1}^2 + \sigma_{g,2}^2 \end{pmatrix}$	$\begin{pmatrix} \sigma_{12}^2 + \sigma_{g,1}^2 + \sigma_{g,2}^2 & \sigma_{g,1}^2 & \sigma_{g,2}^2 \\ \sigma_{g,1}^2 & \sigma_{13}^2 + \sigma_{g,1}^2 + \sigma_{g,3}^2 & \sigma_{g,3}^2 \\ \sigma_{g,2}^2 & \sigma_{g,3}^2 & \sigma_{23}^2 + \sigma_{g,2}^2 + \sigma_{g,3}^2 \end{pmatrix}$

**Table 4.** Log visibility amplitude design and covariance matrices for 2- and 3-station arrays, along with matrices relevant for their construction. Here,  $B = \binom{N}{2}$  is the number of baselines.

This lengthy expression encodes two symmetries of closure phases. The first symmetry is a “cycling invariance,”

$$\psi_{ijk} = \psi_{jki} = \psi_{kij}, \quad (\text{B34})$$

which indicates that the choice of starting baseline doesn’t affect the value of the closure phase. The second symmetry is a sign flip imparted upon reversing the direction of the sequence,

$$\psi_{ijk} = -\psi_{jik}. \quad (\text{B35})$$

These symmetries are illustrated in Figure 16.

As with the visibilities (see Appendix B.1), we can construct a design matrix  $\Psi$  that maps from the visibility phase space to the closure phase space,

$$\psi = \Psi \phi, \quad (\text{B36})$$

where  $\phi$  and  $\psi$  are vectors of visibility phases and closure phases, respectively. This design matrix allows us to express the closure phase covariance matrix  $\Sigma_\psi$  in terms of the visibility phase covariance matrix  $\Sigma_\phi$ ,

$$\Sigma_\psi = \Psi \Sigma_\phi \Psi^\top. \quad (\text{B37})$$

By construction, the closure phases use combinations of visibility phases for which the gain contributions cancel, a property referred to as “phase aberration annihilation” by Lannes (1991). This cancellation manifests in the design matrices as



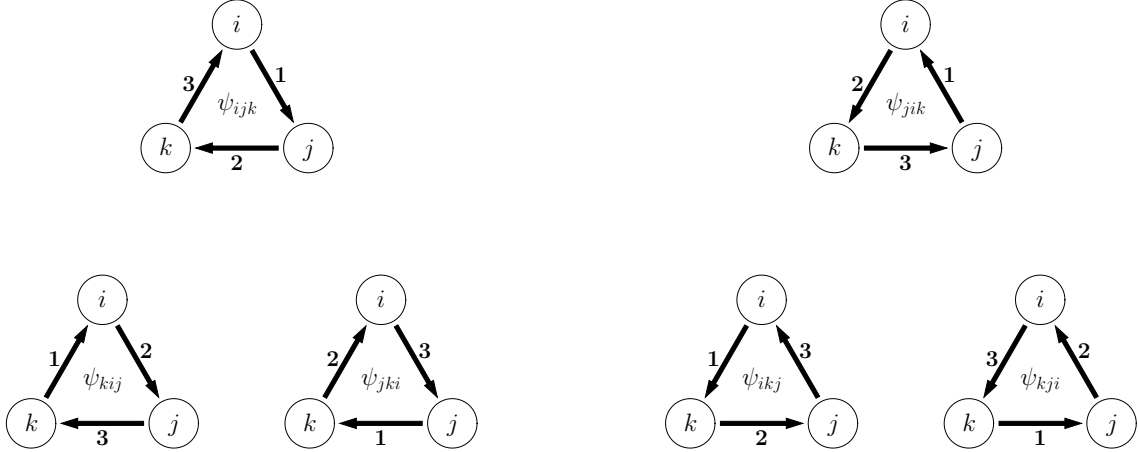


**Figure 16.** Diagrams of closure phase symmetries for a single triangle containing stations  $i$ ,  $j$ , and  $k$ , with baselines numbered in the sequence used to construct the closure phase. All closure phases in the left block of diagrams have the same value, and all closure phases in the right block of diagrams have the same value, but the values corresponding to the two blocks of diagrams differ in sign. The left three diagrams illustrate closure phases constructed in a clockwise manner using a different starting baseline each time; the value of the closure phase is invariant to the choice of starting baseline (Equation B34). The left and right blocks of diagrams differ by a reversal in the direction of closure phase construction; the value of the closure phase changes sign upon direction reversal (Equation B35).

well: the product of closure phase and visibility phase design matrices evaluates to the zero matrix,

$$\Psi \Phi = \mathbf{0}. \quad (\text{B38})$$

We can thus express the closure phase covariance matrix more simply in terms of the diagonal matrix containing only visibility phase thermal variances,

$$\Sigma_{\psi} = \Psi \mathbf{S}_{\psi} \Psi^{\top}. \quad (\text{B39})$$

For a general  $N$ -station array with  $N > 3$ , we present the following recursive relationship for constructing the design matrix corresponding to a maximal set of closure phases:

$$\Psi_{N,\max} = \begin{pmatrix} \Phi_{N-1} & \mathbf{I}_{\binom{N-1}{2}} \\ \mathbf{0} & \Psi_{N-1,\max} \end{pmatrix}, \quad (\text{B40})$$

where  $\Phi_{N-1}$  is the visibility phase design matrix for an array with  $N-1$  stations (see Equation B32),  $\mathbf{0}$  is a  $\binom{N-1}{2} \times (N-1)$  matrix containing only 0's,  $\mathbf{I}_{\binom{N-1}{2}}$  is the identity matrix of rank  $\binom{N-1}{2}$ , and  $\Psi_{N-1,\max}$  is the maximal closure phase design matrix for an array with  $N-1$  stations.

To obtain a minimal (nonredundant) set of closure phases for an  $N$ -station array, we can use a modified design matrix:

$$\Psi_N = \begin{pmatrix} \Phi_{N-1} & \mathbf{I}_{\binom{N-1}{2}} \end{pmatrix}. \quad (\text{B41})$$

Table 5 lists example closure phase design and covariance matrices.

### B.3. Log closure amplitude matrices

A pair of closure quadrangles can have up to two baselines in common, meaning that in general log closure amplitudes will be covariant. The covariance between log closure amplitude measurements  $c_{ijkl}$  and  $c_{mnpq}$  can be expressed as

$$\begin{aligned} \text{Cov}(c_{ijkl}, c_{mnpq}) = & \sigma_{ij}^2 (\delta_{im}\delta_{jn} + \delta_{in}\delta_{jm} + \delta_{ip}\delta_{jq} + \delta_{iq}\delta_{jp}) \\ & - \sigma_{ij}^2 (\delta_{im}\delta_{jp} + \delta_{in}\delta_{jq} + \delta_{ip}\delta_{jm} + \delta_{iq}\delta_{jn}) \\ & + \sigma_{kl}^2 (\delta_{km}\delta_{ln} + \delta_{kn}\delta_{lm} + \delta_{kp}\delta_{lq} + \delta_{kq}\delta_{lp}) \\ & - \sigma_{kl}^2 (\delta_{km}\delta_{lp} + \delta_{kn}\delta_{lq} + \delta_{kp}\delta_{lm} + \delta_{kq}\delta_{ln}) \\ & + \sigma_{ik}^2 (\delta_{im}\delta_{kp} + \delta_{in}\delta_{kq} + \delta_{ip}\delta_{km} + \delta_{iq}\delta_{kn}) \\ & - \sigma_{ik}^2 (\delta_{im}\delta_{kn} + \delta_{in}\delta_{kp} + \delta_{ip}\delta_{km} + \delta_{iq}\delta_{kn}) \\ & + \sigma_{jl}^2 (\delta_{jm}\delta_{lp} + \delta_{jn}\delta_{lq} + \delta_{jp}\delta_{lm} + \delta_{jq}\delta_{ln}) \\ & - \sigma_{jl}^2 (\delta_{jm}\delta_{ln} + \delta_{jn}\delta_{lm} + \delta_{jp}\delta_{lq} + \delta_{jq}\delta_{lp}), \end{aligned} \quad (\text{B42})$$

where  $\sigma_{ij}^2$  is the variance in the log visibility amplitude measurement  $a_{ij}$ . There are three symmetries encoded in the above expression. The first of these is a cycling invariance,

$$c_{ijkl} = c_{lkji}, \quad (\text{B43})$$

indicating that, as for the closure phases, the log closure amplitude value doesn't change with choice of starting baseline. The second symmetry is a direction invariance,

$$c_{ijkl} = c_{klij}, \quad (\text{B44})$$

		Number of stations ( $N$ )					
Matrix	Shape	$N = 3$			$N = 4$		
$\phi^\top$	$1 \times B$	$\begin{pmatrix} \phi_{12} & \phi_{13} & \phi_{23} \end{pmatrix}$			$\begin{pmatrix} \phi_{12} & \phi_{13} & \phi_{14} & \phi_{23} & \phi_{24} & \phi_{34} \end{pmatrix}$		
$\Psi_{\max}$	$T \times B$	$\begin{pmatrix} 1 & -1 & 1 \end{pmatrix}$			$\begin{pmatrix} 1 & -1 & 0 & 1 & 0 & 0 \\ 1 & 0 & -1 & 0 & 1 & 0 \\ 0 & 1 & -1 & 0 & 0 & 1 \\ 0 & 0 & 0 & 1 & -1 & 1 \end{pmatrix}$		
$\Psi$	$t \times B$	$\begin{pmatrix} 1 & -1 & 1 \end{pmatrix}$			$\begin{pmatrix} 1 & -1 & 0 & 1 & 0 & 0 \\ 1 & 0 & -1 & 0 & 1 & 0 \\ 0 & 1 & -1 & 0 & 0 & 1 \end{pmatrix}$		
$\Sigma_{\psi, \max}$	$T \times T$	$\begin{pmatrix} \sigma_{12}^2 + \sigma_{13}^2 + \sigma_{23}^2 \\ \sigma_{12}^2 \\ -\sigma_{13}^2 \\ \sigma_{23}^2 \end{pmatrix}$			$\begin{pmatrix} \sigma_{12}^2 + \sigma_{13}^2 + \sigma_{23}^2 & \sigma_{12}^2 & -\sigma_{13}^2 & \sigma_{23}^2 \\ \sigma_{12}^2 & \sigma_{12}^2 + \sigma_{14}^2 + \sigma_{24}^2 & \sigma_{14}^2 & -\sigma_{24}^2 \\ -\sigma_{13}^2 & \sigma_{14}^2 & \sigma_{13}^2 + \sigma_{14}^2 + \sigma_{34}^2 & \sigma_{34}^2 \\ \sigma_{23}^2 & -\sigma_{24}^2 & \sigma_{34}^2 & \sigma_{23}^2 + \sigma_{24}^2 + \sigma_{34}^2 \end{pmatrix}$		
$\Sigma_{\psi}$	$t \times t$	$\begin{pmatrix} \sigma_{12}^2 + \sigma_{13}^2 + \sigma_{23}^2 \\ \sigma_{12}^2 \\ -\sigma_{13}^2 \end{pmatrix}$			$\begin{pmatrix} \sigma_{12}^2 + \sigma_{13}^2 + \sigma_{23}^2 & \sigma_{12}^2 & -\sigma_{13}^2 \\ \sigma_{12}^2 & \sigma_{12}^2 + \sigma_{14}^2 + \sigma_{24}^2 & \sigma_{14}^2 \\ -\sigma_{13}^2 & \sigma_{14}^2 & \sigma_{13}^2 + \sigma_{14}^2 + \sigma_{34}^2 \end{pmatrix}$		

**Table 5.** Closure phase design and covariance matrices for 3- and 4-element arrays. Here,  $T = \binom{N}{3}$  is the number of triangles in a maximal set,  $t = \binom{N-1}{2}$  is the number of triangles in a minimal set, and  $B = \binom{N}{2}$  is the number of baselines.

showing that, unlike for closure phases, the log closure amplitude value doesn't change when the sequence of baselines is reversed. The third symmetry is a sign flip imparted on the value of the log closure amplitude upon swapping the numerator and denominator,

$$c_{ijkl} = -c_{ikjl}. \quad (\text{B45})$$

These symmetries are illustrated in Figure 17.

We construct a minimal design matrix  $\mathbf{C}$  that maps from the log visibility amplitude space to the log closure amplitude space,

$$\mathbf{c} = \mathbf{C}\mathbf{a}, \quad (\text{B46})$$

where  $\mathbf{a}$  and  $\mathbf{c}$  are vectors of log visibility amplitudes and log closure amplitudes, respectively. This log closure amplitude design matrix is equivalent to the ‘‘amplitude closure operator’’ of Lannes (1990a) and the ‘‘alternate amplitude compilation operator’’ of Lannes (1991). We express the log closure amplitude covariance matrix  $\Sigma_c$  in terms of this design matrix  $\mathbf{C}$  and the log visibility amplitude covariance matrix  $\Sigma_a$ ,

$$\Sigma_c = \mathbf{C}\Sigma_a\mathbf{C}^\top = \mathbf{C}\mathbf{S}_a\mathbf{C}^\top, \quad (\text{B47})$$

where, as with Equation B38, we have used the fact that  $\mathbf{C}\mathbf{A} = \mathbf{0}$  to simplify the construction; this cancellation is referred to as ‘‘amplitude aberration annihilation’’ by Lannes (1991).

For a  $N$ -station array with  $N > 4$ , the design matrix for a minimal set of log closure amplitudes can be constructed using

$$\mathbf{C}_N = \begin{pmatrix} \mathbf{X}_N & \mathbf{Y}_N \\ \mathbf{0} & \mathbf{C}_{N-1} \end{pmatrix}, \quad (\text{B48})$$

where  $\mathbf{C}_{N-1}$  is the design matrix for an array with  $N-1$  stations,  $\mathbf{0}$  is a  $(\frac{(N-1)(N-4)}{2}) \times (N-1)$  matrix of all zeros,

$$\mathbf{X}_N = \begin{pmatrix} \mathbf{I}_{N-2} & -\mathbf{1} \end{pmatrix}, \quad (\text{B49})$$

and  $\mathbf{Y}_N$  is a  $(N-2) \times \binom{N-1}{2}$  matrix constructed by ‘‘cycling’’ through pairs of baselines that don't contain the first station:

$$\mathbf{Y}_N = \begin{pmatrix} 0 & 0 & 0 & \dots & 0 & -1 & 0 & \dots & 0 & 0 & 0 & 0 & 0 & 0 & 0 & 1 \\ -1 & 0 & 0 & \dots & 0 & 0 & 1 & \dots & \cdot & \cdot & \cdot & \cdot & \cdot & \cdot & \cdot & 0 \\ \vdots & & & \ddots & & & & \ddots & & & & & & & & \vdots \\ \cdot & \cdot & \cdot & \dots & \cdot & \cdot & \cdot & \dots & -1 & 0 & 0 & 1 & \cdot & \cdot & \cdot & 0 \\ \cdot & \cdot & \cdot & \dots & \cdot & \cdot & \cdot & \dots & \cdot & \cdot & \cdot & \cdot & -1 & 0 & 1 & \cdot & 0 \\ \cdot & \cdot & \cdot & \dots & \cdot & \cdot & \cdot & \dots & \cdot & \cdot & \cdot & \cdot & \cdot & \cdot & \cdot & -1 & 1 & 0 \end{pmatrix}. \quad (\text{B50})$$

Here, matrix elements represented by a dot indicate zero-valued entries. Table 6 lists example log closure amplitude design and covariance matrices.

### C. WORKED EXAMPLES OF INFORMATION CONTENT

For an array of  $N$  stations, an accounting of the nonredundant closure phases reveals that they differ by an amount  $N-1$  from the number of visibility phases. This offset, which

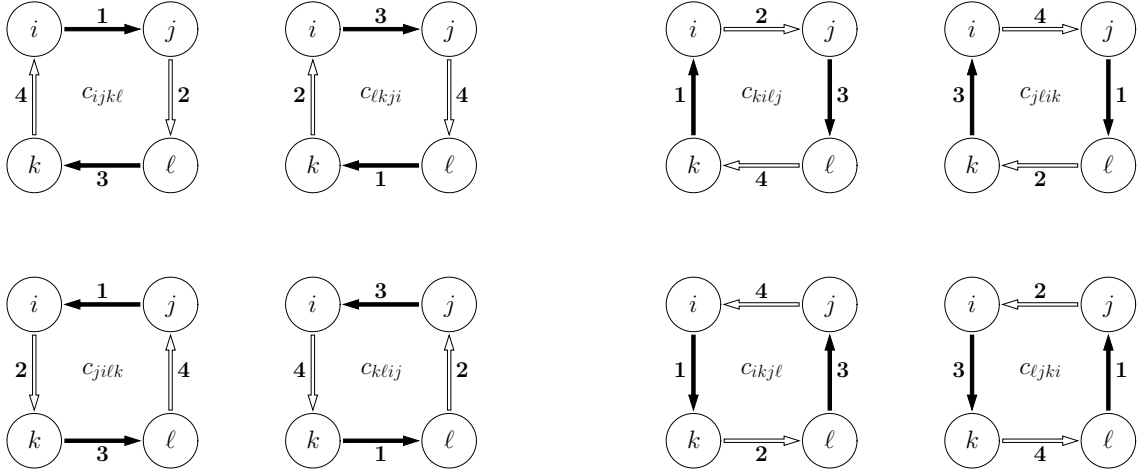


**Figure 17.** Diagrams of log closure amplitude symmetries for a single quadrangle containing stations  $i$ ,  $j$ ,  $k$ , and  $\ell$ , with baselines numbered in the sequence used to construct the log closure amplitude; baselines in the numerator of the closure amplitude are filled in black, while those in the denominator are filled in white. All log closure amplitudes in the left block of diagrams have the same value, and all log closure amplitudes in the right block of diagrams have the same value, but the values corresponding to the two blocks of diagrams differ in sign. Within a single block of diagrams, each row illustrates log closure amplitudes constructed in the same cycle direction but using a different starting baseline; the value of the log closure amplitude is invariant to the choice of starting baseline (Equation B43). Within a single block of diagrams, each column illustrates a reversal in the cycle direction of log closure amplitude construction; the value of the log closure amplitude is invariant upon direction reversal (Equation B44). The left and right blocks of diagrams differ by a swap of numerator and denominator; the value of the log closure amplitude changes sign upon swapping numerator and denominator (Equation B45).

Matrix	Shape	Number of stations ( $N$ )					
		$N = 4$					
$\mathbf{a}^\top$	$1 \times B$	$(a_{12} \ a_{13} \ a_{14} \ a_{23} \ a_{24} \ a_{34})$					
$\mathbf{C}$	$q \times B$	$\begin{pmatrix} 0 & 1 & -1 & -1 & 1 & 0 \\ 1 & 0 & -1 & -1 & 0 & 1 \end{pmatrix}$					
$\Sigma_c$	$q \times q$	$\begin{pmatrix} \sigma_{13}^2 + \sigma_{14}^2 + \sigma_{23}^2 + \sigma_{24}^2 & \sigma_{14}^2 + \sigma_{23}^2 \\ \sigma_{14}^2 + \sigma_{23}^2 & \sigma_{12}^2 + \sigma_{14}^2 + \sigma_{23}^2 + \sigma_{34}^2 \end{pmatrix}$					

**Table 6.** Minimal log closure amplitude design and covariance matrices for 4-element array. Here,  $q = \frac{N(N-3)}{2}$  is the number of quadrangles in a minimal set and  $B = \binom{N}{2}$  is the number of baselines.

is equal to the number of unique gain phases in the array, suggests that closure phases contain all of the source phase information and that the additional degrees of freedom afforded by the visibility phases only describe the gains. A similar situation holds for the closure amplitudes, where the number of nonredundant quadrangles differs from the number of visibility amplitudes by an amount equal to the number of gain amplitudes,  $N$ . In the limit where we have no *a priori* information about the gains, then, the information content in the visibility quantities should be identical to that contained within the closure quantities. In this section we demonstrate the reality of this equality and its lack of dependence on the specific choice of nonredundant closure subset for some selected test cases.

### C.1. Closure phase for $N = 3$ stations

We consider a 3-station interferometer with measured visibility phases ( $\phi_{12}$ ,  $\phi_{13}$ ,  $\phi_{23}$ ) and model visibility phases ( $\hat{\phi}_{12}$ ,  $\hat{\phi}_{13}$ ,  $\hat{\phi}_{23}$ ) related by the station gain phases ( $\hat{\theta}_1$ ,  $\hat{\theta}_2$ ,  $\hat{\theta}_3$ ) as

$$\phi_{ij} = \hat{\phi}_{ij} + \hat{\theta}_i - \hat{\theta}_j. \quad (\text{C51})$$

The information contained in the measured visibilities is captured by their joint likelihood distribution,  $\mathcal{L}$ . If the visibility phases have Gaussian thermal variances ( $\sigma_{12}^2$ ,  $\sigma_{13}^2$ ,  $\sigma_{23}^2$ ), and if we assume that the gain contributions are also Gaussian distributed with variances ( $\sigma_{\theta,1}^2$ ,  $\sigma_{\theta,2}^2$ ,  $\sigma_{\theta,3}^2$ ), then the likeli-

hood of the measured visibility phases can be expressed as a multivariate Gaussian,

$$\mathcal{L} = \frac{1}{\sqrt{(2\pi)^3 \det(\Sigma_\phi)}} \exp \left[ -\frac{1}{2} \tilde{\phi}^\top \Sigma_\phi^{-1} \tilde{\phi} \right], \quad (\text{C52})$$

where

$$\tilde{\phi} = \begin{pmatrix} \phi_{12} - (\hat{\phi}_{12} + \hat{\theta}_1 - \hat{\theta}_2) \\ \phi_{13} - (\hat{\phi}_{13} + \hat{\theta}_1 - \hat{\theta}_3) \\ \phi_{23} - (\hat{\phi}_{23} + \hat{\theta}_2 - \hat{\theta}_3) \end{pmatrix} \equiv \begin{pmatrix} \tilde{\phi}_{12} \\ \tilde{\phi}_{13} \\ \tilde{\phi}_{23} \end{pmatrix} \quad (\text{C53})$$

is the vector of visibility phase residuals and  $\Sigma_\phi$  is the visibility phase covariance matrix (see [Appendix B.1](#)). Because the likelihood is Gaussian and the variances are constant-valued, the quantity

$$\chi_\phi^2 = \tilde{\phi}^\top \Sigma_\phi^{-1} \tilde{\phi} \quad (\text{C54})$$

contains the same information as  $\mathcal{L}$  in a more compact form; we will thus proceed through the use of  $\chi_\phi^2$  rather than  $\mathcal{L}$ .

Our expectation is that in the high-S/N limit – i.e., when the thermal noise is negligible compared to gain variations – the information content in the visibility phases will be identical to that in the closure phases; equivalently,  $\chi_\phi^2$  for the visibility phases should equal  $\chi_\psi^2$  for the closure phases. To simplify the mathematics and notation, let's now suppose that the array is perfectly homogeneous such that we can denote  $\sigma_{\theta,1}^2 = \sigma_{\theta,2}^2 = \sigma_{\theta,3}^2 \equiv \sigma^2$  and  $\sigma_{12}^2 = \sigma_{13}^2 = \sigma_{23}^2 \equiv \varepsilon^2 \sigma^2$ . The high-S/N limit thus corresponds to  $\varepsilon^2 \ll 1$ . To leading order in  $\varepsilon^2$ , we find

$$\Sigma_\phi^{-1} = \frac{1}{3\varepsilon^2 \sigma^2} \begin{pmatrix} 1 & -1 & 1 \\ -1 & 1 & -1 \\ 1 & -1 & 1 \end{pmatrix}, \quad (\text{C55})$$

which corresponds to a  $\chi_\phi^2$  in the same limit of

$$\chi_\phi^2 = \frac{(\tilde{\phi}_{12} - \tilde{\phi}_{13} + \tilde{\phi}_{23})^2}{3\varepsilon^2 \sigma^2}. \quad (\text{C56})$$

Because the array contains only  $N = 3$  stations,  $\binom{N}{3} = \binom{N-1}{2}$  and the complete set of closure phases is equal to the nonredundant set, both of which contain only a single element. We can write the model closure phase as  $\hat{\psi}_{123} = \hat{\phi}_{12} - \hat{\phi}_{13} + \hat{\phi}_{23}$  and the measured closure phase as  $\psi_{123} = \phi_{12} - \phi_{13} + \phi_{23}$ , with corresponding thermal noise given by  $\sigma_{123}^2 = \sigma_{12}^2 + \sigma_{13}^2 + \sigma_{23}^2 = 3\varepsilon \sigma^2$ . The value of  $\chi_\psi^2$  is then written simply as

$$\begin{aligned} \chi_\psi^2 &= \frac{(\psi_{123} - \hat{\psi}_{123})^2}{\sigma_{123}^2} \\ &= \frac{(\tilde{\phi}_{12} - \tilde{\phi}_{13} + \tilde{\phi}_{23})^2}{3\varepsilon^2 \sigma^2}, \end{aligned} \quad (\text{C57})$$

which we can see is identical to [Equation C56](#).

### C.2. Closure phase for $N = 4$ stations

We consider now a 4-station interferometer with measured visibility phases  $(\phi_{12}, \phi_{13}, \phi_{14}, \phi_{23}, \phi_{24}, \phi_{34})$  and model visibility phases  $(\hat{\phi}_{12}, \hat{\phi}_{13}, \hat{\phi}_{14}, \hat{\phi}_{23}, \hat{\phi}_{24}, \hat{\phi}_{34})$  related by the station gain phases  $(\hat{\theta}_1, \hat{\theta}_2, \hat{\theta}_3, \hat{\theta}_4)$  as specified in [Equation C51](#). Following the same procedure as in the previous section, we find in the high-S/N limit that

$$\Sigma_\phi^{-1} = \frac{1}{4\varepsilon^2 \sigma^2} \begin{pmatrix} 2 & -1 & -1 & 1 & 1 & 0 \\ -1 & 2 & -1 & -1 & 0 & 1 \\ -1 & -1 & 2 & 0 & -1 & -1 \\ 1 & -1 & 0 & 2 & -1 & 1 \\ 1 & 0 & -1 & -1 & 2 & -1 \\ 0 & 1 & -1 & 1 & -1 & 2 \end{pmatrix}, \quad (\text{C58})$$

corresponding to

$$\begin{aligned} \chi_\phi^2 &= \frac{(\tilde{\phi}_{12} - \tilde{\phi}_{13} + \tilde{\phi}_{23})^2}{4\varepsilon^2 \sigma^2} + \frac{(\tilde{\phi}_{12} - \tilde{\phi}_{14} + \tilde{\phi}_{24})^2}{4\varepsilon^2 \sigma^2} \\ &+ \frac{(\tilde{\phi}_{13} - \tilde{\phi}_{14} + \tilde{\phi}_{34})^2}{4\varepsilon^2 \sigma^2} + \frac{(\tilde{\phi}_{23} - \tilde{\phi}_{24} + \tilde{\phi}_{34})^2}{4\varepsilon^2 \sigma^2}. \end{aligned} \quad (\text{C59})$$

The 4-station array has 4 closure phases in total, of which 3 are nonredundant. We specify a measured closure phase  $\psi_{ijk}$  as

$$\psi_{ijk} = \phi_{ij} - \phi_{ik} + \phi_{jk}, \quad (\text{C60})$$

with an analogous specification for the corresponding model closure phase  $\hat{\psi}_{ijk}$ . For a particular choice of nonredundant closure phase subset, the value of  $\chi_\psi^2$  will depend on the covariance matrix  $\Sigma_\psi$  for the closure phases (see [Appendix B.2](#) and [Equation B37](#)) and on the vector  $\tilde{\psi}$  of closure phase residuals,

$$\tilde{\psi} = \begin{pmatrix} \psi_{123} - \hat{\psi}_{123} \\ \psi_{124} - \hat{\psi}_{124} \\ \psi_{134} - \hat{\psi}_{134} \end{pmatrix} \equiv \begin{pmatrix} \tilde{\psi}_{123} \\ \tilde{\psi}_{124} \\ \tilde{\psi}_{134} \end{pmatrix}. \quad (\text{C61})$$

After computing the inverse of  $\Sigma_\psi^*$ ,

$$\Sigma_\psi^{-1} = \frac{1}{4\varepsilon^2 \sigma^2} \begin{pmatrix} 2 & -1 & 1 \\ -1 & 2 & -1 \\ 1 & -1 & 2 \end{pmatrix}, \quad (\text{C62})$$

it is a tedious but straightforward algebraic exercise to obtain

$$\begin{aligned} \chi_\psi^2 &= \tilde{\psi}^\top \Sigma_\psi^{-1} \tilde{\psi} \\ &= \frac{\tilde{\psi}_{123}^2 + \tilde{\psi}_{124}^2 + \tilde{\psi}_{134}^2 + \tilde{\psi}_{234}^2}{4\varepsilon^2 \sigma^2}. \end{aligned} \quad (\text{C63})$$

Because closure phases are constructed purely from sums and differences of visibility phases,  $\tilde{\psi}_{ijk} = \tilde{\phi}_{ij} - \tilde{\phi}_{ik} + \tilde{\phi}_{jk}$  and thus Equation C63 is equivalent to Equation C59. Furthermore, Equation C63 no longer shows any signature of the original nonredundant closure phase subset choice; rather, each element of the full redundant set of 4 closure phases is represented equally, and the  $\chi_{\psi}^2$  includes a 3/4 redundancy correction factor (see Equation 38) corresponding to the ratio of linearly independent to total closure phases (note that  $\sigma_{ijk}^2 = 3\varepsilon^2\sigma^2$ ).

### C.3. Closure amplitude for $N = 4$ stations

We consider again a 4-station interferometer with measured log visibility amplitudes ( $a_{12}, a_{13}, a_{14}, a_{23}, a_{24}, a_{34}$ ) and model log visibility amplitudes ( $\hat{a}_{12}, \hat{a}_{13}, \hat{a}_{14}, \hat{a}_{23}, \hat{a}_{24}, \hat{a}_{34}$ ) related by the log station gain amplitudes ( $\hat{g}_1, \hat{g}_2, \hat{g}_3, \hat{g}_4$ ) as

$$\mathbb{E}[a_{ij}] = \hat{a}_{ij} + \hat{g}_i + \hat{g}_j. \quad (\text{C64})$$

As in Appendix C.1, if the measured log visibility amplitudes have Gaussian thermal variances ( $\sigma_{12}^2, \sigma_{13}^2, \sigma_{14}^2, \sigma_{23}^2, \sigma_{24}^2, \sigma_{34}^2$ ) and the log gain amplitude contributions are also Gaussian distributed with variances ( $\sigma_{g,1}^2, \sigma_{g,2}^2, \sigma_{g,3}^2, \sigma_{g,4}^2$ ), then the joint distribution of the measured log visibility amplitudes can be expressed as a multivariate Gaussian. The covariance matrix for this distribution can be constructed using the procedure described in Appendix B.1.

If we once again treat the array as perfectly homogeneous and take the high-S/N limit, then to leading order in  $\varepsilon^2$  we find

$$\Sigma_a^{-1} = \frac{1}{6\varepsilon^2\sigma^2} \begin{pmatrix} 2 & -1 & -1 & -1 & -1 & 2 \\ -1 & 2 & -1 & -1 & 2 & -1 \\ -1 & -1 & 2 & 2 & -1 & -1 \\ -1 & -1 & 2 & 2 & -1 & -1 \\ -1 & 2 & -1 & -1 & 2 & -1 \\ 2 & -1 & -1 & -1 & -1 & 2 \end{pmatrix}. \quad (\text{C65})$$

The corresponding  $\chi_a^2 = \tilde{\mathbf{a}}^\top \Sigma_a^{-1} \tilde{\mathbf{a}}$  can then be written

$$\begin{aligned} \chi_a^2 = & \frac{(\tilde{a}_{12} + \tilde{a}_{34} - \tilde{a}_{13} - \tilde{a}_{24})^2}{6\varepsilon^2\sigma^2} \\ & + \frac{(\tilde{a}_{12} + \tilde{a}_{34} - \tilde{a}_{14} - \tilde{a}_{23})^2}{6\varepsilon^2\sigma^2} \\ & + \frac{(\tilde{a}_{13} + \tilde{a}_{24} - \tilde{a}_{14} - \tilde{a}_{23})^2}{6\varepsilon^2\sigma^2}. \end{aligned} \quad (\text{C66})$$

The 4-station array has 3 closure amplitudes in total, of which 2 are nonredundant. We specify a measured log closure amplitude  $c_{ijk\ell}$  as

$$c_{ijk\ell} = a_{ij} + a_{k\ell} - a_{ik} - a_{j\ell}, \quad (\text{C67})$$

with an analogous specification for the corresponding model log closure amplitude  $\hat{c}_{ijk\ell}$ . For a particular choice of nonredundant closure amplitude subset, the value of  $\chi_c^2$  will depend on the covariance matrix  $\Sigma_c$  for the log closure amplitudes (see Appendix B.3 and Equation B47) and on the vector  $\tilde{\mathbf{c}}$  of log closure amplitude residuals,

$$\tilde{\mathbf{c}} = \begin{pmatrix} c_{1234} - \hat{c}_{1234} \\ c_{1243} - \hat{c}_{1243} \end{pmatrix} \equiv \begin{pmatrix} \tilde{c}_{1234} \\ \tilde{c}_{1243} \end{pmatrix}. \quad (\text{C68})$$

Written out more explicitly, the covariance matrix is given by

$$\Sigma_c = 2\varepsilon^2\sigma^2 \begin{pmatrix} 2 & 1 \\ 1 & 2 \end{pmatrix}, \quad (\text{C69})$$

with corresponding inverse

$$\Sigma_c^{-1} = \frac{1}{6\varepsilon^2\sigma^2} \begin{pmatrix} 2 & -1 \\ -1 & 2 \end{pmatrix}. \quad (\text{C70})$$

We thus obtain

$$\begin{aligned} \chi_c^2 &= \tilde{\mathbf{c}}^\top \Sigma_c^{-1} \tilde{\mathbf{c}} \\ &= \frac{\tilde{c}_{1234}^2 + \tilde{c}_{1243}^2 + \tilde{c}_{1342}^2}{6\varepsilon^2\sigma^2}, \end{aligned} \quad (\text{C71})$$

which is equal to Equation C66. As with the closure phases, we see that the initial choice of minimal log closure amplitude subset has no bearing on the value of  $\chi_c^2$ , and accounts for the redundancy factor of total versus linearly independent closure amplitudes.

### C.4. Closure quantities for arbitrary $N$

We introduce the notion of “mixed phases” that retain all of the information contained in the visibility phases but separate it into two components: one component that is captured by the closure phases and a second component that captures the remaining station-based effects. For an array with  $N$  stations, the mixed phase design matrix operates on the  $B$  baseline phases and is given by

$$\begin{aligned} \Psi_+ &= \begin{pmatrix} \mathbf{I}_{N-1,B} \\ \Psi_N \end{pmatrix} \\ &= \begin{pmatrix} \mathbf{I}_{N-1} & \mathbf{0} \\ \Phi_{N-1} \mathbf{I}_{\binom{N-1}{2}} \end{pmatrix}. \end{aligned} \quad (\text{C72})$$

$\mathbf{I}_{N-1,B}$  is a  $(N-1) \times B$  “rectangular identity matrix” that extracts the first  $N-1$  baseline phases by combining  $\mathbf{I}_{N-1}$ , a standard square identity matrix of rank  $N-1$ , with  $\mathbf{0}$ , a  $(N-1) \times (B-N+1)$  matrix of all zeros.  $\Psi_N$  is the minimal closure phase design matrix for  $N$  stations (see Equation B41), which can be expanded into the visibility phase



design matrix  $\Phi_{N-1}$  for  $N-1$  stations (see Equation B32) and a standard square identity matrix of rank  $\binom{N-1}{2}$ . This design matrix maps from the visibility phase space to the mixed phase space,

$$\psi_+ = \Psi_+ \phi. \quad (\text{C73})$$

For example, the mixed phase design matrix for an array with  $N = 4$  stations is given by

$$\Psi_+ = \begin{pmatrix} 1 & 0 & 0 & 0 & 0 & 0 \\ 0 & 1 & 0 & 0 & 0 & 0 \\ 0 & 0 & 1 & 0 & 0 & 0 \\ 1 & -1 & 0 & 1 & 0 & 0 \\ 1 & 0 & -1 & 0 & 1 & 0 \\ 0 & 1 & -1 & 0 & 0 & 1 \end{pmatrix}, \quad (\text{C74})$$

and the corresponding mixed phase vector is

$$\psi_+ = \begin{pmatrix} \phi_{12} \\ \phi_{13} \\ \phi_{14} \\ \phi_{12} - \phi_{13} + \phi_{23} \\ \phi_{12} - \phi_{14} + \phi_{24} \\ \phi_{13} - \phi_{14} + \phi_{34} \end{pmatrix}. \quad (\text{C75})$$

The mixed phase covariance matrix is given by

$$\Sigma_{\psi_+} = \Psi_+ \Sigma_{\phi} \Psi_+^{\top}. \quad (\text{C76})$$

Using the inverse of the mixed phase design matrix,

$$\Psi_+^{-1} = \begin{pmatrix} \mathbf{I}_{N-1} & \mathbf{0} \\ -\Phi_{N-1} & \mathbf{I}_{\binom{N-1}{2}} \end{pmatrix}, \quad (\text{C77})$$

we can invert Equation C76 to obtain an expression for the visibility phase covariance matrix in terms of the mixed phase covariance matrix,

$$\Sigma_{\phi} = \Psi_+^{-1} \Sigma_{\psi_+} \Psi_+^{\top -1}, \quad (\text{C78})$$

where we note that the inverse transpose is equal to the transposed inverse for the mixed phase design matrix. We can use the above to substitute for  $\Sigma_{\phi}$  in our expression for the visibility phase  $\chi^2$  (see Equation C54),

$$\begin{aligned} \chi_{\phi}^2 &= \tilde{\phi}^{\top} \Sigma_{\phi}^{-1} \tilde{\phi} \\ &= \tilde{\phi}^{\top} \left( \Psi_+^{-1} \Sigma_{\psi_+} \Psi_+^{\top -1} \right)^{-1} \tilde{\phi} \\ &= \tilde{\phi}^{\top} \left( \Psi_+^{\top} \Sigma_{\psi_+}^{-1} \Psi_+ \right) \tilde{\phi} \\ &= (\Psi_+ \tilde{\phi})^{\top} \Sigma_{\psi_+}^{-1} (\Psi_+ \tilde{\phi}) \\ &= \tilde{\psi}_+^{\top} \Sigma_{\psi_+}^{-1} \tilde{\psi}_+, \end{aligned} \quad (\text{C79})$$

revealing that the  $\chi^2$  constructed from mixed phases is equal to that constructed from visibility phases, when all covariances are taken into account. This is due to the fact that the mixed phases are generated through a nonsingular linear transformation of the visibility phases.

To see how the mixed phases reduce to purely closure phases in the high-S/N limit, it is convenient to consider the following decomposition of the mixed phase covariance matrix,

$$\Sigma_{\psi_+} = \begin{pmatrix} \Sigma'_{\phi} & \mathbf{W}^{\top} \\ \mathbf{W} & \Sigma_{\psi} \end{pmatrix}, \quad (\text{C80})$$

where  $\Sigma'_{\phi}$  is the first  $(N-1) \times (N-1)$  upper left subset of the full visibility phase covariance matrix  $\Sigma_{\phi}$ ,  $\Sigma_{\psi}$  is the closure phase covariance matrix, and  $\mathbf{W} = \Phi_{N-1} \mathbf{S}'_{\phi}$  is the covariance between the closure phases and the first  $N-1$  visibility phases. Since the closure phases are independent of station gain, both  $\mathbf{W}$  and  $\Sigma_{\psi}$  include only baseline thermal noise.

Using a strategy analogous to that employed in the previous sections, where parameter  $\varepsilon^2 \sim \mathcal{O}(\sigma_{ij}^2 / \sigma_{\theta,i}^2)$  relates statistical error in visibility phase to that from gain uncertainty, we examine the behavior of  $\Sigma_{\psi_+}^{-1}$  as  $\varepsilon \rightarrow 0$ . The sub-matrices of  $\Sigma_{\psi_+}$  scale with  $\varepsilon$  as

$$\begin{aligned} \Sigma'_{\phi} &\propto 1 \\ \mathbf{W} &\propto \varepsilon^2 \\ \Sigma_{\psi} &\propto \varepsilon^2. \end{aligned}$$

From the block matrix form of Equation C80, we can write the inverse mixed phase covariance matrix as

$$\begin{aligned} \Sigma_{\psi_+}^{-1} &= \begin{pmatrix} \left( \Sigma'_{\phi} - \mathbf{W}^{\top} \Sigma_{\psi}^{-1} \mathbf{W} \right)^{-1} \\ -\Sigma_{\psi}^{-1} \mathbf{W} \left( \Sigma'_{\phi} - \mathbf{W}^{\top} \Sigma_{\psi}^{-1} \mathbf{W} \right)^{-1} \\ -\left( \Sigma'_{\phi} - \mathbf{W}^{\top} \Sigma_{\psi}^{-1} \mathbf{W} \right)^{-1} \mathbf{W}^{\top} \Sigma_{\psi}^{-1} \\ \Sigma_{\psi}^{-1} + \Sigma_{\psi}^{-1} \mathbf{W} \left( \Sigma'_{\phi} - \mathbf{W}^{\top} \Sigma_{\psi}^{-1} \mathbf{W} \right)^{-1} \mathbf{W}^{\top} \Sigma_{\psi}^{-1} \end{pmatrix}. \end{aligned} \quad (\text{C81})$$

These four sub-matrices scale with  $\varepsilon$  as

$$\begin{aligned} \left( \Sigma'_{\phi} - \mathbf{W}^{\top} \Sigma_{\psi}^{-1} \mathbf{W} \right)^{-1} &\propto 1 \\ \left( \Sigma'_{\phi} - \mathbf{W}^{\top} \Sigma_{\psi}^{-1} \mathbf{W} \right)^{-1} \mathbf{W}^{\top} \Sigma_{\psi}^{-1} &\propto 1 \\ \Sigma_{\psi}^{-1} \mathbf{W} \left( \Sigma'_{\phi} - \mathbf{W}^{\top} \Sigma_{\psi}^{-1} \mathbf{W} \right)^{-1} &\propto 1 \\ \Sigma_{\psi}^{-1} + \Sigma_{\psi}^{-1} \mathbf{W} \left( \Sigma'_{\phi} - \mathbf{W}^{\top} \Sigma_{\psi}^{-1} \mathbf{W} \right)^{-1} \mathbf{W}^{\top} \Sigma_{\psi}^{-1} &\propto \frac{1}{\varepsilon^2}, \end{aligned}$$

and we can see that the  $\Sigma_{\psi}^{-1}$  term in the lower right sub-matrix dominates  $\Sigma_{\psi_+}^{-1}$ . The product of  $\Sigma_{\psi_+}^{-1}$  with  $\tilde{\psi}_+$  in this limit

will therefore serve to isolate the last  $t$  terms of  $\tilde{\psi}_+$  (which are just the closure phases  $\tilde{\psi}$ ), and multiply them by  $\Sigma_{\tilde{\psi}}^{-1}$ :

$$\begin{aligned} \lim_{\varepsilon \rightarrow 0} (\chi_\phi^2) &= \tilde{\psi}^\top \Sigma_{\tilde{\psi}}^{-1} \tilde{\psi} \\ &= \chi_{\tilde{\psi}}^2. \end{aligned} \quad (\text{C82})$$

The final result is that the visibility phase  $\chi^2$ , in the limit where the uncertainty in the baseline-based quantities is much smaller than the uncertainty in the station-based quantities, is equal to the closure phase  $\chi^2$ .

The equivalence between  $\chi_a^2$  derived from a complete set of log-visibility amplitudes in the  $\varepsilon \rightarrow 0$  limit and  $\chi_c^2$  derived from log-closure amplitudes is demonstrated the same way. Here the corresponding design matrix and mixed log-amplitudes are,

$$\mathbf{C}_+ = \begin{pmatrix} \mathbf{I}_{N,B} \\ \mathbf{C}_N \end{pmatrix} \quad \mathbf{c}_+ = \mathbf{C}_+ \mathbf{a}, \quad (\text{C83})$$

which draws from the first  $N$  visibility log-amplitudes followed by a minimal set of log-closure amplitudes. The transformation to mixed quantities is nonsingular so long as the first  $N$  baselines drawn do not form any closed quadrangles (or that the first  $N-1$  baselines do not form any closed triangles, in the case of mixed phases). This condition is met by the baseline ordering convention used in this paper. The reduction in Equations C80–C82 then follows under substitution of phase with log-amplitude quantities.

### C.5. Explicit gain marginalization

In the previous Sections C.1–C.4, we have shown that the information content in closure quantities is equivalent to that in the baseline visibilities for the limit of completely unconstrained gains, so long as the covariance structure of the corresponding observables is taken into account. We now relate the use of covariance in the residual visibility likelihood construction (Equation C52) to explicit analytic marginalization over Gaussian uncertainties in phase or log amplitude station gain. Thus, in the limit of completely unconstrained gains, use of closure quantities should give identical results to explicit numerical marginalization over all possible gains; and, for the case of finite Gaussian uncertainties in phase or log amplitude station gain, use of the residual visibility covariance should give identical results to explicit numerical marginalization over Gaussian priors for the gains.

For an array with  $N$  stations under modeled gain corrections, we can write Equation C64 for all baselines using

$$\mathbf{E}[\tilde{\mathbf{a}}] = \mathbf{E}[\mathbf{a}] - \hat{\mathbf{a}} = \mathbf{A}(\mathbf{g} - \hat{\mathbf{g}}) = \mathbf{A}\tilde{\mathbf{g}}, \quad (\text{C84})$$

where  $\mathbf{A}\tilde{\mathbf{g}}$  is a residual vector of log visibility amplitude correction factors. For example, a 3-station array would have

$$\mathbf{A}\tilde{\mathbf{g}} = \begin{pmatrix} 1 & 1 & 0 \\ 1 & 0 & 1 \\ 0 & 1 & 1 \end{pmatrix} \begin{pmatrix} \tilde{g}_1 \\ \tilde{g}_2 \\ \tilde{g}_3 \end{pmatrix} = \begin{pmatrix} \tilde{g}_1 + \tilde{g}_2 \\ \tilde{g}_1 + \tilde{g}_3 \\ \tilde{g}_2 + \tilde{g}_3 \end{pmatrix}. \quad (\text{C85})$$

The Gaussian likelihood for calibrated log visibility amplitudes is then expressed as

$$p(\tilde{\mathbf{a}}|\tilde{\mathbf{g}}) = \frac{1}{\sqrt{\det(2\pi\mathbf{S}_a)}} \exp \left[ -\frac{1}{2} (\tilde{\mathbf{a}} - \mathbf{A}\tilde{\mathbf{g}})^\top \mathbf{S}_a^{-1} (\tilde{\mathbf{a}} - \mathbf{A}\tilde{\mathbf{g}}) \right], \quad (\text{C86})$$

where we note that  $\mathbf{S}_a$  contains only baseline thermal noise and is diagonal.

If we further impose independent zero-mean Gaussian priors on each of the model gain correction factors, we can express the joint prior as

$$p(\tilde{\mathbf{g}}) = \frac{1}{\sqrt{\det(2\pi\mathbf{\Sigma}_g)}} \exp \left[ -\frac{1}{2} \tilde{\mathbf{g}}^\top \mathbf{\Sigma}_g^{-1} \tilde{\mathbf{g}} \right]. \quad (\text{C87})$$

We can use this prior to marginalize the log visibility amplitudes over the log gain amplitudes,

$$\mathcal{L}_a = \int p(\tilde{\mathbf{a}}|\tilde{\mathbf{g}}) p(\tilde{\mathbf{g}}) d\tilde{\mathbf{g}}, \quad (\text{C88})$$

where  $\mathcal{L}_a$  represents the marginalized likelihood.

The integrand in Equation C88 is a product of exponentials, which together contain several terms that depend on  $\tilde{\mathbf{g}}$ . To evaluate the integral, we would like to consolidate these terms. By defining

$$\mathbf{M} = \mathbf{M}^\top \equiv \mathbf{A}^\top \mathbf{S}_a^{-1} \mathbf{A} + \mathbf{\Sigma}_g^{-1} \quad (\text{C89})$$

$$\boldsymbol{\mu} \equiv \mathbf{A}^\top \mathbf{S}_a^{-1} \tilde{\mathbf{a}}, \quad (\text{C90})$$

completing the square, and then pulling terms that don't depend on  $\tilde{\mathbf{g}}$  out of the integral, we obtain

$$\begin{aligned} \mathcal{L}_a &= \frac{1}{\sqrt{\det(2\pi\mathbf{S}_a) \det(2\pi\mathbf{\Sigma}_g)}} \\ &\times \exp \left[ -\frac{1}{2} (\tilde{\mathbf{a}}^\top \mathbf{S}_a^{-1} \tilde{\mathbf{a}} - \boldsymbol{\mu}^\top \mathbf{M}^{-1} \boldsymbol{\mu}) \right] \\ &\times \int \exp \left[ -\frac{1}{2} (\tilde{\mathbf{g}} - \mathbf{M}^{-1} \boldsymbol{\mu})^\top \mathbf{M} (\tilde{\mathbf{g}} - \mathbf{M}^{-1} \boldsymbol{\mu}) \right] d\tilde{\mathbf{g}}. \end{aligned} \quad (\text{C91})$$

The integrand now contains only a single multivariate Gaussian in  $\tilde{\mathbf{g}}$ , with mean  $\mathbf{M}^{-1} \boldsymbol{\mu}$  and covariance  $\mathbf{M}^{-1}$ . Integrating over all  $\tilde{\mathbf{g}}$  thus yields the volume  $\sqrt{\det(2\pi\mathbf{M}^{-1})}$ , so that

$$\mathcal{L}_a = \frac{1}{\sqrt{\det(2\pi\mathbf{S}_a) \det(2\pi\mathbf{\Sigma}_g) \det(\mathbf{M}/2\pi)}} \times \exp \left[ -\frac{1}{2} \left( \tilde{\mathbf{a}}^\top \mathbf{S}_a^{-1} \tilde{\mathbf{a}} - \boldsymbol{\mu}^\top \mathbf{M}^{-1} \boldsymbol{\mu} \right) \right]. \quad (\text{C92})$$

Upon expanding  $\boldsymbol{\mu}^\top \mathbf{M}^{-1} \boldsymbol{\mu}$  and directly applying the Woodbury matrix inverse identity we obtain,

$$\mathcal{L}_a = \frac{1}{\sqrt{\det(2\pi\mathbf{S}_a) \det(2\pi\mathbf{\Sigma}_g) \det(\mathbf{M}/2\pi)}} \times \exp \left[ -\frac{1}{2} \tilde{\mathbf{a}}^\top \left( \mathbf{S}_a + \mathbf{A} \mathbf{\Sigma}_g \mathbf{A}^\top \right)^{-1} \tilde{\mathbf{a}} \right], \quad (\text{C93})$$

where we have obtained the log visibility amplitude covariance  $\mathbf{\Sigma}_a = \mathbf{S}_a + \mathbf{A} \mathbf{\Sigma}_g \mathbf{A}^\top$  analogous to [Equation B31](#).

For the determinants in the normalization constant,

$$\det(\mathbf{M}/2\pi) \det(2\pi\mathbf{\Sigma}_g) \det(2\pi\mathbf{S}_a) \quad (\text{C94})$$

$$= \det \left( \mathbf{A}^\top \mathbf{S}_a^{-1} \mathbf{A} \mathbf{\Sigma}_g + \mathbf{I} \right) \det(2\pi\mathbf{S}_a) \quad (\text{C95})$$

$$= \det \left( \mathbf{A} \mathbf{\Sigma}_g \mathbf{A}^\top \mathbf{S}_a^{-1} + \mathbf{I} \right) \det(2\pi\mathbf{S}_a) \quad (\text{C96})$$

$$= \det \left( 2\pi(\mathbf{A} \mathbf{\Sigma}_g \mathbf{A}^\top + \mathbf{S}_a) \right). \quad (\text{C97})$$

Here, we have used the Weinstein-Aronszajn matrix identity  $\det(\mathbf{I} + \mathbf{X}\mathbf{Y}) = \det(\mathbf{I} + \mathbf{Y}\mathbf{X})$ . The marginalized likelihood can thus be written as

$$\mathcal{L}_a = \frac{1}{\sqrt{\det(2\pi\mathbf{\Sigma}_a)}} \exp \left[ -\frac{1}{2} \tilde{\mathbf{a}}^\top \mathbf{\Sigma}_a^{-1} \tilde{\mathbf{a}} \right], \quad (\text{C98})$$

showing that the marginalization over Gaussian priors in log gain amplitude is fully captured through the use of visibility covariance as in [Equation C52](#). The derivation applies to any linear transformation of independent Gaussian observables. In particular it is the same for partially known visibility phases under the substitution  $(\mathbf{a}, \mathbf{A}, \mathbf{g}) \rightarrow (\boldsymbol{\phi}, \boldsymbol{\Phi}, \boldsymbol{\theta})$ .